Institutionen för fysik

Thermodynamics of microscopic environments
From anomalous diffusion to heat engines

Aykut Argun
Institutionen för Fysik
Göteborgs Universitet

Akademisk avhandling för filosofie doktorsexamen i fysik, som med tillstånd från Naturvetenskapliga fakulteten kommer att offentligt försvaras måndagen den 14.06.2021 kl. 14 i PJ-salen, institutionen för fysik, Fysikgården 2b, Göteborg.

ISBN: 978-91-8009-384-2 (tryckt version)
ISBN: 978-91-8009-385-9 (elektronisk version)
Tillgänglig via http://hdl.handle.net/2077/68298

Thermodynamics of microscopic environments

From anomalous diffusion to heat engines

Aykut Argun
Institutionen för Fysik
Göteborgs Universitet

Sammanfattning

Till skillnad från deras makroskopiska motsvarigheter utvecklas inte mikroskopiska system deterministiskt på grund av inverkan från termiskt brus. Sådana system är föremål för fluktuationer som endast kan studeras inom ramen för stokastisk termodynamik. Under de senaste decennierna har utvecklingen av stokastisk termodynamik lett till mikroskopiska värmemotorer, icke-jämviktsförhållanden, studien av avvikande diffusion och aktiv Brownskrörelse.

I denna avhandling visar jag experimentellt att icke-Boltzmann-statistik dyker upp i system som är kopplade till ett aktivt bad. Denna icke-Boltzmann-statistik som härrör från korrelerat aktivt brus stör också icke jämvikts förhållandena. Ändå visar jag att dessa relationer kan återställas med en effektiv potential metod. Därefter demonstrerar jag en experimentell implementation av en mikroskopisk värmemotor. Denna motor, som kallas för den Brownska-gyratorn, är kopplad till två olika värmebad längs vinkelräta riktningar. Jag visar att när den är innesluten i en elliptisk fälla som inte är anpassad till temperaturanisotropin, är den Brownska partikeln utsatt för ett vridmoment på grund av symmetribrottet. Detta vridmoment skapar en autonom motor vars riktning och amplitud kan kontrolleras genom att justera orienteringen på den elliptiska fällan. Sedan visar jag att de kraftfält som verkar på Browniska partiklar kan kalibreras med en datadriven metod som överträffar de befintliga kalibreringsmetoderna. Än viktigare, jag visar att den här metoden, med namnet DeepCalib, kan kalibrera icke-konservativa och tidsvarierande kraftfält för vilka det saknas standardiserade kalibreringsmetoder. Slutligen visar jag att en liknande metod baserad på maskininlärning kan användas för att karakterisera avvikande diffusion från enstaka banor. Denna metod, kallad RANDI, är mycket mångsidig och fungerar bra i olika uppgifter inklusive klassificering, skattning och segmentering av avvikande diffusion.

Arbetet som presenteras i denna avhandling presenterar nya experiment som främjar mikroskopisk termodynamik samt nyutvecklade metoder vilka öppnar upp nya möjligheter att analysera stokastiska banor. Dessa resultat har ökat den vetenskapliga kunskapen i sambanden mellan mikroskopisk termodynamik, avvikande diffusion, aktiv materia och maskininlärning.

Nyckelord: avvikande diffusion, mikroskopisk termodynamik, värmemotorer, djupinlärning, dataanalys, aktiv materia

Thesis for the degree of Doctor of Philosophy

Thermodynamics of microscopic environments

From anomalous diffusion to heat engines

Aykut Argun

Department of Physics
University of Gothenburg

Gothenburg, Sweden 2021

UNIVERSITY OF GOTHENBURG

Thermodynamics of microscopic environments
From anomalous diffusion to heat engines

Aykut Argun
978-91-8009-384-2 (printed)
978-91-8009-385-9 (electronic)

Department of Physics
University of Gothenburg
SE-412 96 Göteborg
Tel: +46 (0)31-7721000, Fax: +46 (0)31-7723496
htttp://www.physics.gu.se

Printed by STEMA SPECIALTRYCK AB
Gothenburg, Sweden 2021

Thermodynamics of microscopic environments

From anomalous diffusion to heat engines

Aykut Argun
Department of Physics
University of Gothenburg

Abstract

Unlike their macroscopic counterparts, microscopic systems do not evolve deterministically due to the thermal noise becoming prominent. Such systems are subject to fluctuations that can only be studied within the framework of stochastic thermodynamics. Within the last few decades, the development of stochastic thermodynamics has lead to microscopic heat engines, nonequilibrium relations and the study of anomalous diffusion and active Brownian motion.

In this thesis, I experimentally show that the non-Boltzmann statistics emerge in systems that are coupled to an active bath. These non-Boltzmann statistics that result from correlated active noise also disturb the nonequilibrium relations. Nevertheless, I show that these relations can be recovered using an effective potential approach. Next, I demonstrate an experimental realization of a microscopic heat engine. This engine is referred to as the Brownian gyrator, which is coupled to two different heat baths along perpendicular directions. I show that when confined into an elliptical trap that is not aligned with the temperature anisotropy, the Brownian particle is subject to a torque due to the symmetry breaking. This torque creates an autonomous engine whose direction and amplitude can be controlled by tuning the alignment of the elliptical trap. Then, I show that the force fields acting on Brownian particles can be calibrated using a data-driven method that outperforms the existing calibration methods. More importantly, I show that this method, named DeepCalib, can calibrate non-conservative and time-varying force fields that no standard calibration methods exist. Finally, I show that a similar machine-learning-based approach can be used to characterize anomalous diffusion from single trajectories. This method, named RANDI, is very versatile and performs very well in various tasks including classification, inference and segmentation of anomalous diffusion.

The work presented in this thesis presents novel experiments that advance microscopic thermodynamics as well as newly developed methods that open up new possibilities in analyzing stochastic trajectories. These findings increased the scientific knowledge at the nexus between microscopic thermodynamics, anomalous diffusion, active matter and machine learning.

Keywords: microscopic thermodynamics, anomalous diffusion, heat engines, deep learning, calibration, data analysis, active bath

The publications that are included in the context of this thesis:

Paper I: Non-Boltzmann stationary distributions and nonequilibrium relations in active baths

Aykut Argun, AliReza Moradi, Ercag Pince, Gokhan Baris Bagci, Alberto Imparato and Giovanni Volpe

Physical Review E 94.6 (2016): 062150

Paper II: Experimental realization of a minimal microscopic heat engine

Aykut Argun, Jalpa Soni, Lennart Dabelow, Stefano Bo, Guiseppe Pesce, Ralf Eicchorn and Giovanni Volpe

Physical Review E 96.5 (2017): 052106

Paper III: Enhanced force-field calibration via machine learning

Aykut Argun, Tobias Thalheim, Stefano Bo, Frank Cichos and Giovanni Volpe

Applied Physics Reviews 7.4 (2020): 041404.

Paper IV: Classification, inference and segmentation of anomalous diffusion with recurrent neural networks

Aykut Argun, Giovanni Volpe and Stefano Bo

arXiv preprint arXiv:2104.00553 (2021).

Additional publications that are not included in the context of this thesis:

Paper V: Better stability with measurement errors

Aykut Argun and Giovanni Volpe

Journal of Statistical Phyiscs 163.6 (2016): 1477-1485

Paper VI: Digital video microscopy enhanced by deep learning

Saga Helgadottir, **Aykut Argun** and Giovanni Volpe

Optica **6**, 506-513 (2019)

Paper VII: Quantitative Digital Microscopy with Deep Learning

Benjamin Midtvedt, Saga Helgadottir, **Aykut Argun**, Jesús Pineda, Daniel Midtvedt and Giovanni Volpe

Applied Physics Reviews 8.1 (2021): 011310.

Contents

CHAPTER 1

Introduction

1.1 Brownian motion and optical trapping

Understanding the physics of tiny particles is very important for research on cells, nanotechnology and soft matter physics. Microscopic objects are subject to continuous random collisions from the surrounding molecules when they are suspended in a liquid or gas environment. These collisions create a random force acting on these microscopic objects that constantly changes its value and direction, which is known as thermal noise. As a result of the thermal noise, small particles in liquid or air environment undergo a random motion that is known as diffusion. This phenomenon is also referred to as Brownian motion, which takes its name from Robert Brown, a botanist that observed diffusion within pollen grains in water in 1827.

Brownian motion of a microscopic particle (also referred to as a Brownian particle) can be mathematically expressed by the following formula:

$$m\frac{d^2x}{dt^2} = -\gamma\frac{dx}{dt} + \sqrt{2k_\mathrm{B}T\gamma}W_x(t) \tag{1.1}$$

where γ represents the friction in the medium, T represents the temperature of the environment and W_x represents an uncorrelated random term that creates the stochasticity [1, 2]. An example motion of a Brownian particle is shown in Fig. 1.1(a). At very short timescales (microseconds, inset in Fig. 1.1(a)), this motion shows a ballistic behaviour due to the particles inertia, while at longer timescales it becomes completely random. As can be seen from the example trajectory (and unlike macroscopic objects), microscopic particles do not have a completely deterministic motion due to the random parameters in their equation of motion (Eq. 1.1), which results in a different outcome for each realization. Nevertheless, it can still be characterized by ensemble averages using statistics.

An important measure of Brownian motion is mean-squared-displacement (MSD) that is expressed in the following way:

$$\mathrm{MSD}(t) = \langle [x(t+\tau) - x(\tau)]^2 \rangle \tag{1.2}$$

where $\langle \cdot \rangle$ represents the ensemble averaging over many realizations. An example MSD of a Brownian particle is shown in Fig. 1.1(b). The MSD scales with

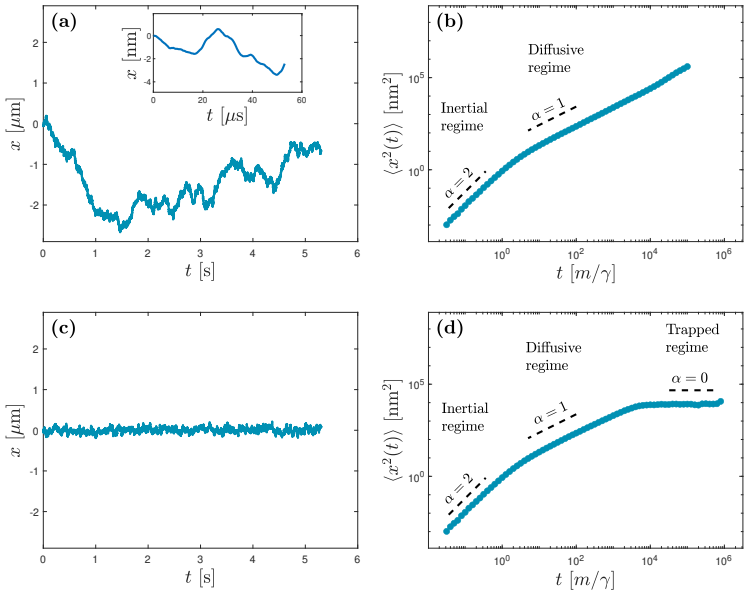

Figure 1.1: **Brownian motion and optical trapping. (a)** Simulation of a free Brownian particle (R=1 μm, $m = 10^{-13}$ g) in a liquid environment. The particle's trajectory x is completely random at long timescales, although its inertia is observable at shorter (inertial) time scales (inset). **(b)** The mean square displacement of the free particle (Eq. 1.2) has an exponent of $\alpha = 2$ (ballistic motion) at inertial time scales ($t \ll m/\gamma$) and $\alpha = 1$ (diffusive motion) for longer time scales ($t \gg m/\gamma$). **(c)** Simulated trajectory of the same Brownian particle in an optical trap ($k = 10^{-6}$ N/m). The optical trap confines the diffusion into a small region around the trapping point. **(d)** The mean square displacement of the trapped particle (Eq. 1.2) reaches to a finite limit where it becomes constant ($\alpha = 0$, trapped regime) due to the confinement of the particle by the optical trap.

t^2 at very short time scales (inertial regime, Fig. 1.1(b)) when the particle conserves its velocity, while it scales with t in larger time scales (diffusive regime, Fig. 1.1(b)) when its motion becomes completely random. In the large t limit, the MSD for a spherical Brownian particle will take the form [3]:

$$\mathrm{MSD}(t) = \frac{k_\mathrm{B}T}{3\pi\eta R}\, t \tag{1.3}$$

where η is the viscosity of the environment and R is the radius of the particle. Importantly, the diffusion of the particle is inversely proportional to its radius, which means that the Brownian motion becomes a lot stronger as the particles get smaller. Specifically, the time it takes for a particle to diffuse on the order of its own size (the time (t) when MSD(t) is proportional to R^2) scales with R^3, as MSD$\propto R^{-1}$. This makes extremely difficult to make observations on small particles in a liquid environment under microscope, such as synthetic colloids, bacteria, cells and biomolecules. Fortunately, it is possible to confine Brownian

motion by taking advantage of optical forces as proposed by Arthur Ashkin [4, 5]. Ashkin showed that by focusing a laser beam using a high numerical aperture objective, one can create a high intensity focal spot that can trap particles with optical forces in liquid, air or even vacuum. This can be applied to cells [6], bacteria [7], synthetic microparticles [4] and even individual atoms [8]. Optical trapping has revolutionized biophysics, cell biology, nanotechnology, microscopic thermodynamics and soft matter physics since its discovery [9], leading to the inventors receiving the Nobel prize in Physics in 2018 [10].

A particle placed in an optical trap is subject to a restoring force that is proportional to its displacement from the focal spot. This creates a harmonic trapping potential where Brownian particles can be trapped [5]. A typical trajectory of an optically trapped Brownian particle is shown in Fig. 1.1(c). As it can be seen from this trajectory, although fluctuations arise due to thermal forces, the particle is not allowed to leave the trapping region. This behaviour is also reflected in the particle's MSD (Fig. 1.1(d)) that does not increase beyond the value that it asymptotically converges. Stabilizing such small particles in place permits scientists to make extended measurements for their properties in their natural liquid environment. In addition, optical tweezers permit us to measure forces that are as small as femtonewtons, which has helped to experimentally prove a great number of fundamental theories in the thermodynamics of small systems [11].

1.2 Microscopic thermodynamics

Microscopic thermodynamics deals with the relation between thermodynamic observables (such as work and free energy) of microscopic particles when the system is driven out of equilibrium. In order to understand the details of non-equilibrium physics of Brownian particles, their equilibrium behaviour needs to be observed first. Therefore, we can start by considering a Brownian particle confined within a potential well $U(x)$. In this case, the particle's equation of motion will have the form:

$$m\frac{d^2x}{dt^2} = -\gamma\frac{dx}{dt} - \frac{dU(x)}{dx} + \sqrt{2k_\mathrm{B}T\gamma}W_x(t) \tag{1.4}$$

If the Brownian particle is micron-sized and it is immersed in water, the viscous forces are dominant over the inertial forces so the inertial term ($m\ddot{x}$) can be neglected [12]. Therefore, we obtain the overdamped version of Eq. (1.4):

$$\frac{dx}{dt} = -\frac{1}{\gamma}\frac{dU(x)}{dx} + \sqrt{2k_\mathrm{B}T/\gamma}W_x(t) \tag{1.5}$$

Although there are significant challenges to numerically solve stochastic differential equations, particularly related with the infinite variance of white noise, it is possible to solve Eq. (1.5) with finite difference methods [3, 13, 14]. By numerically simulating Eq. (1.5), I obtained trajectories for various potentials, shown in Fig. 1.2(d-f). Eq. (1.5) is called the overdamped Langevin equation [13] and we will be dealing with this equation in the rest of this chapter.

Equilibrium distribution and detailed balance

Eq. (1.5) can also be solved analytically by using the Fokker-Planck equation [15]:

$$\partial_t P(x,t) = \frac{1}{\gamma}\partial_x \left(\frac{dU(x)}{dx} P(x,t) \right) + \frac{k_\mathrm{B}T}{\gamma}\partial_x^2 P(x,t) \tag{1.6}$$

where $P(x,t)$ denotes the probability density function of the particle as a function of x and t. For equilibrium, we are looking for a stationary solution where the particle has thermalized ($\partial_t P(x,t) = 0$), i.e., when P is a function of x only. If this is the case, the left hand side of Eq. (1.6) vanishes and we obtain:

$$-\partial_x \left(\frac{dU(x)}{dx} P_{eq}(x) \right) = k_\mathrm{B}T \partial_x^2 P_{eq}(x)$$

$$-\frac{dU(x)}{dx} P_{eq}(x) = k_\mathrm{B}T \partial_x P_{eq}(x) + C$$

$$P_{eq}(x) = \frac{1}{Z} \exp\left(-\frac{U(x)}{k_\mathrm{B}T} \right) \tag{1.7}$$

where $Z = \int \exp\left(-\frac{U(x)}{k_\mathrm{B}T}\right)$ is the partition function. Eq. 1.7 can also be written using the Helmholtz free energy $F = -k_\mathrm{B}T\log(Z)$:

$$P_{eq}(x) = \exp\left(-\frac{U(x) - F}{k_\mathrm{B}T} \right) \tag{1.8}$$

This distribution is called the Boltzmann distribution. A Brownian particle subject to thermal noise will reach the Boltzmann distribution when it is confined in any stable potential well. I also verify this relation numerically from the distribution of the data obtained by simulating Eq. (1.5) for various potentials, as shown in Fig. 1.2(g-i). In **Paper I** [16], I also verify experimentally that a Brownian particle in a harmonic optical trapping potential follows the Boltzmann distribution, as the starting point to explore the probability distributions of microscopic particles in active baths.

In dimensions higher than one, having a steady-state distribution, however, is not enough for a system to be in equilibrium. The system should not have any probability current, therefore the probability of forward and backward transitions between any two states should be the same. Consider two of the available states S_1 and S_2 with energies U_1 and U_2, the transition rates in both directions should be the same:

$$p_1(t)p\left[S_2(t+\Delta t) \mid S_1(t)\right] = p_2(t)p\left[S_1(t+\Delta t) \mid S_2(t)\right]$$

$$\exp\left(\frac{-U_1}{k_\mathrm{B}T}\right) p\left[S_2(t+\Delta t) \mid S_1(t)\right] = \exp\left(\frac{-U_2}{k_\mathrm{B}T}\right) p\left[S_1(t+\Delta t) \mid S_2(t)\right] \tag{1.9}$$

this relation is called detailed balance [17] and requires equal rate of transitions between the two states. Therefore, we can find the rate of conditional probabilities that represent a forward and backward transition:

$$\frac{p\left[S_2(t+\Delta t) \mid S_1(t)\right]}{p\left[S_1(t+\Delta t) \mid S_2(t)\right]} = \exp\left(\frac{-(U_2 - U_1)}{k_\mathrm{B}T}\right) \tag{1.10}$$

I will make use of this equation when I will explain Crooks fluctuation theorem.

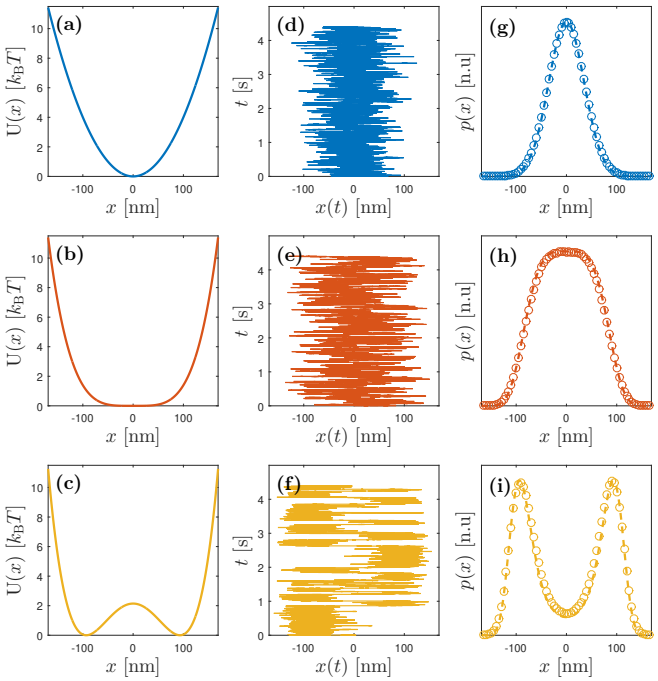

Figure 1.2: **Demonstration of Boltzmann distribution for a confined Brownian particle. (a)**,**(b)** and **(c)**: Various confining potentials such as a harmonic potential (a), a quartic potential (b), and a bistable potential (c) are shown. **(d)**, **(e)** and **(f)**: Corresponding simulated trajectories of a colloidal particle with radius $R = 1$ μm under the confining potentials shown in (a), (b), and (c), respectively. Trajectories are obtained by numerically solving Eq. (1.5). Matlab code is provided in the appendix B. **(g)**, **(h)** and **(i)**: Resulting numerical probability distributions (circles) of the particles obtained from trajectories, which are in perfect agreement with the theoretical probability ditributions (solid lines) given by Eq. (1.7)

Stochastic Energetics

The thermodynamics of microscopic systems are very different from that of their macroscopic counterparts. The fundamental difference between the two, is that the observable quantities (such as heat, work or free energy) for macroscopic systems are much larger (typically by a factor of at least $\approx 10^{20}$) than $k_{\mathrm{B}}T$ so that the thermal fluctuations do not matter. However, when we consider a single microscopic particle, the rules of macroscopic thermodynamics do not apply, although they still hold in average [18].

Consider a Brownian particle confined in a potential $U(x)$, which is not a function of time but only the position of the particle. Since we do not change the parameters of the system, we do not perform work on the particle in this case. However, due to fluctuations, the particle is still constantly exchanging energy with the surrounding heat bath. In other words, when the particle

climbs up the confining potential with Brownian motion, it borrows energy from the surrounding water molecules. This means that the change in the particle's potential energy comes from the surrounding heat bath:

$$dU = dQ$$

In a more general scenario, the heat transferred from the thermal bath to the particle can be written as [18]:

$$dQ = \frac{\partial U(x)}{\partial x} dx \tag{1.11}$$

Unlike macroscopic systems, Brownian particles cannot be isolated from their heat baths because they are immersed in their environment and are constantly in contact with the water molecules that surround them. Therefore, it is not straightforward to realize an adiabatic process on colloids [19].

Now, consider that the confining potential also depends on a control parameter $\lambda(t)$ that is time dependent. In this case, we are also going to perform work on the Brownian particle as we change the control parameter:

$$U = U(x, \lambda(t))$$

$$dU = \underbrace{\frac{\partial U(x, \lambda(t))}{\partial x} dx}_{dQ} + \frac{\partial U(x, \lambda(t))}{\partial \lambda} d\lambda \tag{1.12}$$

The first law of thermodynamics states [18]:

$$dU = dQ + dW \tag{1.13}$$

Combining Eq. (1.13) and Eq. (1.12) yields:

$$dW = \frac{\partial U(x, \lambda(t))}{\partial \lambda} d\lambda \tag{1.14}$$

Therefore, we do thermodynamics work on the Brownian particle by changing the parameters of the potential energy. Eq. 1.14 and Eq. 1.11 provide us with a framework for theoretical studies in microscopic thermodynamics, first introduced by Sekimoto [20]. Eq. 1.13 assures that this notation satisfies the first law of thermodynamics. The second law, however, is not always satisfied for microscopic systems [21]. This phenomenon got a lot of researchers interested and similar results for different microscopic systems were found by a number of groups [22–25]. Even though the second law can no longer be taken for granted for microscopic thermodynamics, it has been shown that it still holds in average [20].

I numerically demonstrate a simple non-equilibrium thermodynamic process for a microscopic particle in Fig. 1.3, while the particle is in an optical trap with a varying stiffness over time. In this example, the temperature of the environment is kept constant (isothermal process) while the stiffness of the trap is raised from $k_\mathrm{i} = 1$ pN/μm (Fig. 1.3(a)) to $k_\mathrm{f} = 1$ pN/μm (Fig. 1.3(b)). Some of the sample trajectories from different realizations of the same protocol are

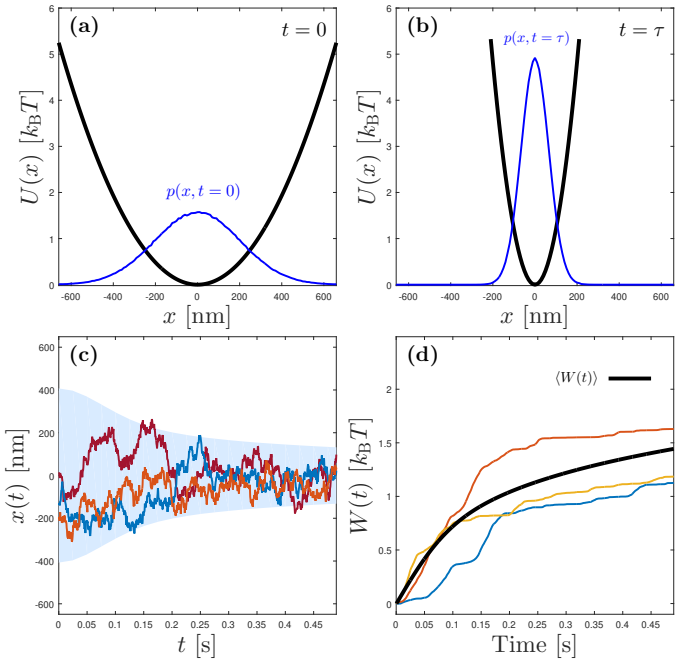

Figure 1.3: **Demonstration of a thermodynamic process for a microscopic particle.** **(a)**: The initial potential well and the initial probability distribution of the particle are shown. **(b)**: The final potential and the final probability distribution of the particle are shown, the process takes $\tau = 0.5$ s time. **(c)**: Several sample trajectories of a Brownian particle in a harmonic trap which undergoes an isothermal compression. Note that different realizations of the same non-equilibrium protocols yield significantly different trajectories. The particle's standart deviation over time is calculated over 1000000 realizations and indicated with the light blue background shading. **(d)**: Work done on the trajectories that are shown in (c). Average work done is also shown by black line. Note that in such a stochastic process, fluctuations around the mean value are significant.

shown in Fig. 1.3(c). Evidently, (unlike macroscopic systems) the microscopic particle follows a different trajectory each time, leading to a work that changes for each realization, as shown in Fig. 1.3(d). This is because of the thermal fluctuations that are play a prominent role in the microscopic world as I will explain in detail in the next section.

The first thermodynamic heat engine was proposed by Sadi Carnot in 1824 [26]. These heat engines became progressively smaller with the advancement of technology during the 20-th century. After the fundamentals of microscopic thermodynamics were established, scientists discovered methods to convert thermal energy into work even for micro-scale systems with only a few degrees of freedom. Ideas of such engines started with Brownian ratchets [27] that couple physical asymmetries of the system with thermal asymmetries in order to create propulsion or rotation. These were followed by the first realization of a micron-sized Stirling engine [28, 29] and Carnot engine [30]. In **Paper II** [31], I demonstrate how we experimentally realized a Brownian gyrator [32] that is both externally controllable and autonomous. I show that the Brownian gyrator is capable of extracting work with a minimal degree of complexity while being in simultaneous contact with two heat baths.

Fluctuation theorems

Observations of the violation of the second law of thermodynamics [21] triggered substantial follow up research in the field of stochastic thermodynamics. Due to the fact that fluctuations play a prominent role, a single stochastic trajectory would behave in a way that is not allowed by the second law of thermodynamics. In other words, a microscopic thermodynamic system might produce negative entropy during limited time. However, the second law of thermodynamics still holds on average [20]. This is due to the fact that the probability of producing negative entropy is lower than the probability of producing positive entropy. In fact, it has been shown that these probabilities relate to each other with an equality for microscopically reversible systems, such as a Brownian particle [33]. In this section, I will illustrate some fundamental fluctuation theorems, namely Crooks fluctuation theorem, the Jarzynski equality and the integral fluctuation theorem.

I will start by considering a Brownian particle in a thermal bath driven by an overdamped Langevin equation. Such a system is Markovian as the particle's future trajectory has no dependence on its history. I assume that the particle is initially held in a potential of the following form:

$$U(x) = U(x, \lambda_0) \tag{1.15}$$

where λ_0 is the initial value of a control parameter that can be driven externally. We start changing this control parameter at $t = t_0$ and end the process at $t = t_N$. Without loss of generality, we can change $\lambda(t)$ in a discrete manner:

$$\Lambda_F \equiv \lambda_0 \underset{t=t_0}{\Longrightarrow} \lambda_1 \cdots \lambda_n \underset{t=t_n}{\Longrightarrow} \lambda_{n+1} \cdots \lambda_N \underset{t=t_N}{\Longrightarrow} \lambda_{N+1} \quad . \tag{1.16}$$

The limit $N \to \infty$ corresponds to the continous case. I denote a certain trajectory, X as follows:

$$X = X\left(x_0(t_0), x_1(t_1), ...x_n(t_n).....x_{N-1}(t_{N-1}), x_N(t_N)\right) \tag{1.17}$$

Given that the particle is initially at x_0 at $t = t_0$, the probability of observing the trajectory X can be written as a product of conditional probabilities:

$$P_{\mathrm{F}}(X) = p\left[x_1(t_1) \mid x_0(t_0)\right]_{\lambda_1} \cdots p\left[x_n(t_n) \mid x_{n-1}(t_{n-1})\right]_{\lambda_n} \cdots p\left[x_N(t_N) \mid x_{N-1}(t_{N-1})\right]_{\lambda_N} \tag{1.18}$$

Now consider that I operate the time-reversed protocol Λ_B, which starts with λ_{N+1} and ends with λ_0, opposite to Λ_F:

$$\Lambda_B \equiv \lambda_{N+1} \underset{t=t_0}{\Longrightarrow} \lambda_N \cdots \lambda_{n+1} \underset{t=t_n}{\Longrightarrow} \lambda_n \cdots \lambda_1 \underset{t=t_N}{\Longrightarrow} \lambda_0 \quad . \tag{1.19}$$

It is possible to write down explicitly the probability to observe the reversed trajectory under the reversed protocol. Similar to Eq. (1.18), we can express this probability given that the particle initially starts at x_N:

$$P_{\mathrm{R}}(\tilde{X}) = p\left[x_{N-1}(t_{N-1}) \mid x_N(t_N)\right]_{\lambda_N} \cdots p\left[x_{n-1}(t_{n-1}) \mid x_n(t_n)\right]_{\lambda_n} \cdots p\left[x_0(t_0) \mid x_1(t_1)\right]_{\lambda_1} \tag{1.20}$$

$$= p\left[x_0(t_0) \mid x_1(t_1)\right]_{\lambda_1} \cdots p\left[x_{n-1}(t_{n-1}) \mid x_n(t_n)\right]_{\lambda_n} \cdots p\left[x_{N-1}(t_{N-1}) \mid x_N(t_N)\right]_{\lambda_N} \tag{1.21}$$

Now we can calculate the rate of the probabilities of observing the time reversed trajectory under the time reversed protocol:

$$\frac{P_{\mathrm{F}}(X)}{P_{\mathrm{R}}(\tilde{X})} = \frac{p\left[x_1(t_1) \mid x_0(t_0)\right]_{\lambda_1}}{p\left[x_0(t_0) \mid x_1(t_1)\right]_{\lambda_1}} \cdots \frac{p\left[x_n(t_n) \mid x_{n-1}(t_{n-1})\right]_{\lambda_n}}{p\left[x_{n-1}(t_{n-1}) \mid x_n(t_n)\right]_{\lambda_n}} \cdots \frac{p\left[x_N(t_N) \mid x_{N-1}(t_{N-1})\right]_{\lambda_N}}{p\left[x_{N-1}(t_{N-1}) \mid x_N(t_N)\right]_{\lambda_N}}$$

Each fraction in the above equation is the rate between the forward and backward transitions between two states under the same control parameter. If the system is Markovian and therefore independent from its history, this ratio of probabilities will be the same as if the particle were in equilibrium. In other words, if the particle is known to be at a certain position at a certain time, it is not important whether it has been in equilibrium or not for a Markovian system. Therefore, each fraction in the above expression can be replaced by the energy difference between the initial and final energies of the particle according to Eq. (1.10):

$$\frac{P_{\mathrm{F}}(X)}{P_{\mathrm{R}}(\tilde{X})} = \underbrace{\frac{p\left[x_1(t_1) \mid x_0(t_0)\right]_{\lambda_1}}{p\left[x_0(t_0) \mid x_1(t_1)\right]_{\lambda_1}}}_{\exp(-\beta Q_1)} \cdots \underbrace{\frac{p\left[x_n(t_n) \mid x_{n-1}(t_{n-1})\right]_{\lambda_n}}{p\left[x_{n-1}(t_{n-1}) \mid x_n(t_n)\right]_{\lambda_n}}}_{\exp(-\beta Q_n)} \cdots \underbrace{\frac{p\left[x_N(t_N) \mid x_{N-1}(t_{N-1})\right]_{\lambda_N}}{p\left[x_{N-1}(t_{N-1}) \mid x_N(t_N)\right]_{\lambda_N}}}_{\exp(-\beta Q_N)} \tag{1.22}$$

$$\frac{P_{\mathrm{F}}(X)}{P_{\mathrm{R}}(\tilde{X})} = \exp\left[-\beta(Q_1 + Q_2 + Q_3 + ... + Q_N)\right] \tag{1.23}$$

which leads to:

$$\frac{P_F(X(t), \lambda(t) \mid x(t_0) = x_0)}{P_R(\tilde{X}(t), \tilde{\lambda}(t) \mid x(t_0) = x_N)} = e^{-\beta Q}$$

where $Q = Q_1 + Q_2 + Q_3 + ... + Q_N$ is the total heat transfer from the thermal bath to the particle during the forward protocol. Note that this equation holds if the initial position is set to x_0 in the forward and x_N in the backward process.

If the systems are initially thermalized, we have to multiply the probability of the initial position of the required trajectory:

$$\frac{P_F(X(t),\lambda(t))}{P_R(\tilde{X}(t),\tilde{\lambda}(t))} = e^{-\beta Q}\frac{p_{eq}(x_0,\lambda_0)}{p_{eq}(x_N,\lambda_{N+1})} = e^{-\beta Q}\frac{\exp(-\beta(U(x_0,\lambda_0)-F_i)}{\exp(-\beta(U(x_N,\lambda_{N+1})-F_f)} \tag{1.24}$$

which leads to:

$$\frac{P_F(X(t),\lambda(t))}{P_R(\tilde{X}(t),\tilde{\lambda}(t))} = e^{\beta(\Delta U - Q - \Delta F)} = e^{\beta(W-\Delta F)} \tag{1.25}$$

This means that all the trajectories that yield the same work in a non-equilibrium process are equally likely to be reversed under time-reversed protocol if the system is initially thermalized. Therefore, I arrive at the work fluctuation theorem [33]:

$$\frac{P_F(+W)}{P_R(-W)} = e^{\beta(W-\Delta F)} \tag{1.26}$$

Eq. 1.26 is a very powerful equality in order to calculate free energy differences between different microscopic states, even from a few repetitions of a forward and backward thermodynamic protocol. It has been used, for example, to measure the free energy differences of RNA folding [34] and reconstruct free energy profiles of DNA hairpins [35]. I will now numerically demonstrate the use of this equality in an example.

Consider a Brownian particle ($R = 1$ μm) that is held in a potential that transitions from a double-well to a single-well trap:

$$U(x,\lambda(t)) = \frac{Kx^4}{4}\lambda(t) + \frac{kx^2}{2}(1-2\lambda(t)) \tag{1.27}$$

where $U(x,\lambda(t))$ represents the potential energy, $K = 1.05\times10^8$ N/m^3) and $k = 3.64\times10^{-6}$ N/m) are coefficients representing the cubic and linear forces. I assume that the control parameter $\lambda(t)$ linearly decreases from $\lambda(0) = 1$ to $\lambda(\tau) = 0$ during a time span of τ, resulting in a transition from a double-well well into a single-well. I remark that this is a completely random choice that I fancy, this example would work for any arbitrary protocol. I call this protocol the forward process (Fig. 1.4(a)) and the time reversed version of this protocol ($\lambda(0) = 0$ to $\lambda(\tau) = 1$) the backward process (Fig. 1.4(a)). I start the simulation at $t = -2$, meaning that the particle has a relaxation time of 2 seconds in the initial potential before the protocol begins. I repeat this experimental protocol 10 million times and I calculate the work I apply on the particle (Eq. 1.14) each time in the forward and backward processes. This provides me a very smooth distribution of the work applied during forward (solid lines) and backward (dashed lines). I repeat this numerical experiment with different speeds, specifically $\tau = 200$ ms (red lines), $\tau = 50$ ms (red lines) and $\tau = 20$ ms (red lines). I show that the applied work and the extracted work distributions ($P_F(W)$ and $P_R(-W)$) of the forward and backward processes overlap less as the process is executed faster (τ is smaller), which means it becomes less reversible, as shown in Fig. 1.4. However, $P_F(W)$ and $P_R(-W)$ are always equal at $W = \Delta F$ (dashed black line). Finally, the ratio of $P_F(W)$

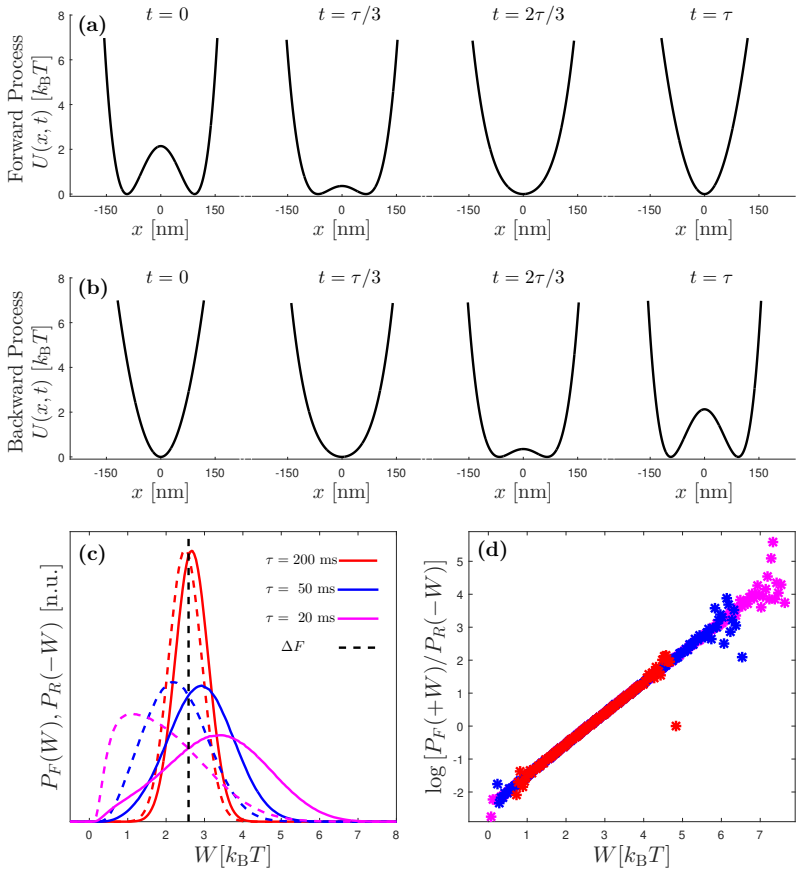

Figure 1.4: **Numerical demonstration of Crooks fluctuation theorem in an arbitrary process. (a)** The forward protocol is demonstrated: Initially the particle is held in a bistable potential and the potential changes into a harmonic potential within time τ. **(b)** The backward protocol is demonstrated: this is the opposite of the protocol. **(c)** Resulting work distributions in the forward (solid lines) and backward (dashed lines) processes for different driving time τ. Note that no matter how fast we operate the process, $P_F(+W)$ and $P_R(-W)$ are equal at the value of the change in free energy ΔF (black dashed line). **(d)** The rate of probabilities of the applied work in the forward protocol and extracted work in the backward protocol. For various durations of the protocol, Eq. (1.26) is verified. Work distributions are obtained by repeating the protocols 10 million times.

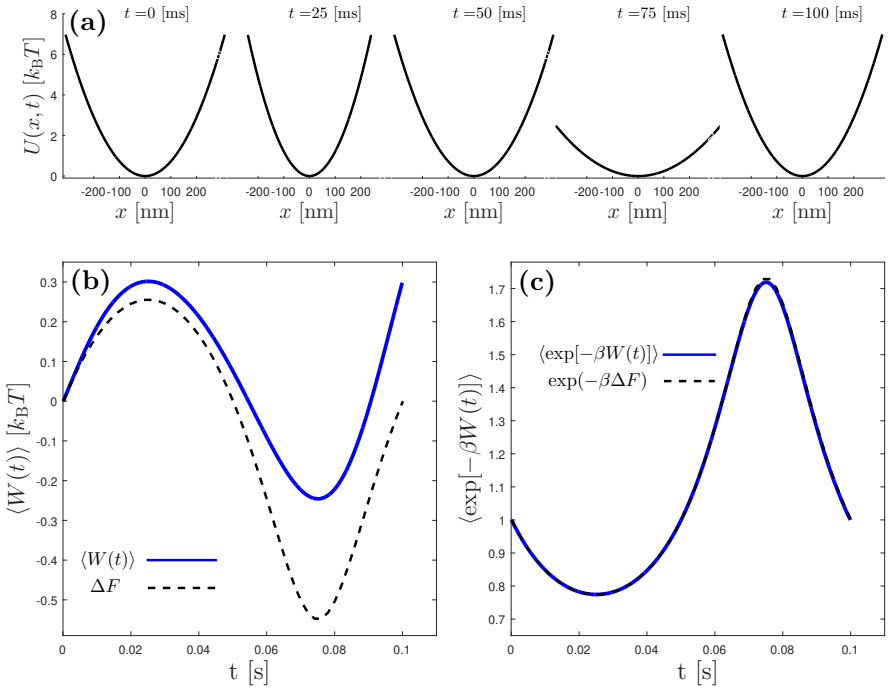

Figure 1.5: **Numerical demonstration of Jarzynski equality in a time-dependent harmonic trap. (a)** The protocol of the nonequilibrium process. The stiffness (k) is subject to a sinusoidal change with a period of 100 milliseconds. **(b)** The average work applied as a function of time during the process described in (a). Note that in average, I apply greater work than the change in free energy in an irreversible process, which is in agreement with the second law. **(c)** Numerical presentation of Jarzynski equality. The Boltzmann weighted exponential average of the work applied follows exactly the Boltzmann weighted exponential of the change in free energy. The work values are averages over 100000 realizations of the same protocol.

and $P_R(-W)$ perfectly obeys Eq. 1.26 independent from how irreversible to process is, as shown in Fig. 1.4(d).

An important implication of Eq. 1.26 is the Jarzynski equality, although it can be derived in multiple different ways [36, 37]. In order to demonstrate Jarzynski equality, I will calculate the exponential average of the applied work in a nonequilibrium process ($\langle \exp(-\beta W) \rangle$) using Eq. 1.26:

$$\langle \exp(-\beta W) \rangle = \int \exp(-\beta W)\, P_F(W) dW$$

Here, $P_F(W)$ is the probability of applying the work W along the forward non-equilibrium process. I will substitute $P_F(W)$ from Eq. (1.26):

$$\langle \exp(-\beta W) \rangle = \int \exp(-\beta W)\, P_R(-W) \exp[\beta(W - \Delta F)]\, dW \qquad (1.28)$$

$$= \int \exp\left(-\beta \Delta F\right) P_R(-W) dW \tag{1.29}$$

Note that $\exp\left(-\beta \Delta F\right)$ is constant, and can be moved out of the integral. The rest of the right hand side is a probability integral that equals unity according to normalization. Therefore, we arrive at the Jarzynski equality:

$$\langle \exp\left(-\beta W\right) \rangle = \exp\left(-\beta \Delta F\right) \tag{1.30}$$

.

Eq. 1.30 [36] is a remarkable theoretical that allows us to recover free energies from non-equilibrium trajectories. Therefore, it is no surprise that this equation helped many scientists to experimentally measure free energies such as stretching RNA molecules [38], individual titin molecules [39], defects in diamonds [40], trapped ion systems [41], small friction forces [42] and electronic systems [43]. I will now demonstrate the use of Jarzynski equality with a numerical example.

I consider a Brownian particle ($R = 1$ μm) held in a harmonic potential with an oscillating stiffness:

$$U(x, \lambda(t)) = \frac{1}{2} k[3 + 2\sin(\omega t)]x^2 \tag{1.31}$$

where the stiffness is subject to a sinusoidal change ($\omega = 20\pi$) between k (0.2 fN/μm) and $5k$ (1 fN/μm). This process is shown in Fig. 1.5(a). The applied work on the particle is averaged over 100000 realizations of the same protocol. As it can be seen in in Fig. 1.5(b), the average applied work on the particle is higher than the free energy change, which is in agreement with the second law. Unfortunately, the second law allows us to only predict an upper bound for the free energy change, even if we have many measurements. Exponential average of the work applied using the left hand side of Eq. (1.30), however, agrees perfectly with the exponential change of the free energy ($\exp\left(-\beta \Delta F\right)$), as shown in Fig. 1.5(c). Therefore, the free energy difference can be calculated if the distribution of the work from a nonequilibrium process is known.

As I have numerically shown, both Eq. 1.26 and Eq. 1.30 are very useful for estimating free energies from non-equilibrium processes. However, in **Paper II** [31], I show that this is not true for systems that are coupled to an active environment. We also show that this is due to the non-Gaussian distributions in the trapping potential due to the properties of the active bath, which makes the assumption in Eq. 1.24 invalid. Nevertheless, I show these nonequilibrium relations can still be recovered by considering the effective potential potential energy that satisfies the Gaussian distribution of the steady state [16].

1.3 Anomalous diffusion

So far, everything I have discussed was driven by standard Brownian motion, which is considered Markovian. This means that the particle's future trajectory depends only on its current state, not on the location history. In addition, the standard Brownian motion is also ergodic, which means that the ensemble average and time average yield the same results. However, many systems show

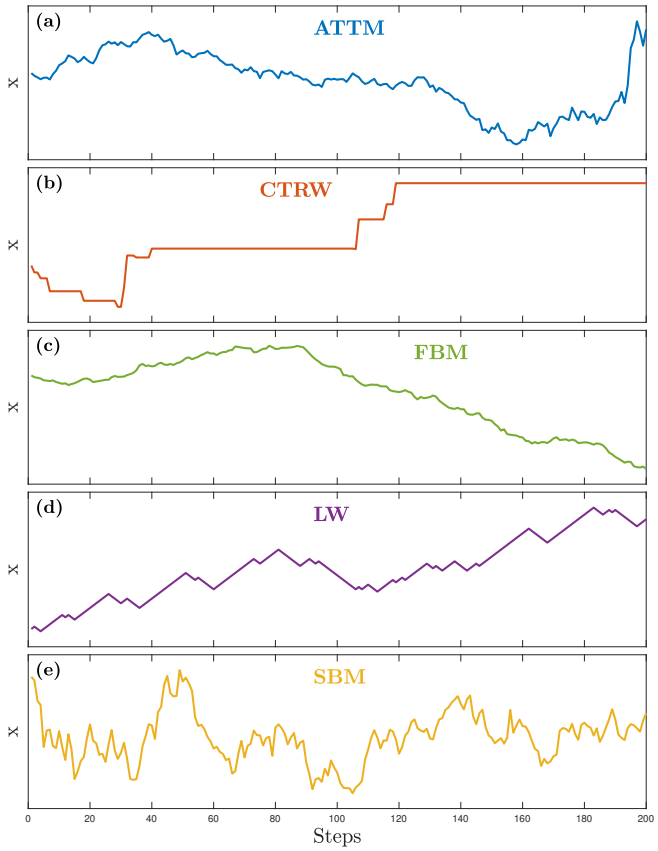

Figure 1.6: **Anomalous diffusion models.** Sample trajectories of anomalous diffusion including (a) annealed transient time motion (ATTM), (b) continous time random walk (CTRW), (c) fractional Brownian motion (FBM), (d) Levy walk (LW) and (e) scaled Brownian motion (SBM).

present diffusive dynamics that deviate from this behavior. Examples include the intracellular environment, foraging animals, particles in turbulent flows or financial time series [44–47]. These anomalous diffusion systems exhibit different kinds of diffusion dynamics than can be discontinuous, non-Markovian or non-ergodic. Importantly, anomalous diffusion is not always driven by uncorrelated noise that is Markovian, which leads to the violation of thermodynamic relations for various cases [48]. These systems are instrinsically out of equilibrium and can only be treated within the framework of nonequilibrium thermodynamics [27, 49–52]. In this section, I will discuss the properties of different types of anomalous diffusion and their properties.

There are several models to describe different kinds of anomalous diffusion behaviour [47]. An important measure of an anomalous diffusion trajectory is its MSD (Eq. 1.2), where the exponent α indicates the growth of MSD with time (MSD$\propto t^{\alpha}$). Unlike the regular diffusion where the exponent of the anomalous

diffusion is $\alpha = 1$, anomalous diffusion trajectories might have an exponent that is smaller ($\alpha < 1$) or larger ($\alpha > 1$), which are referred to as sub-diffusion and super-diffusion, respectively. I am going to describe some of the most commonly used anomalous diffusion models:

Annealed transient time motion (ATTM): This is a Brownian motion with random changes in the diffusion coefficient [53]. The waiting times have the probability distribution of the form $p(\delta t) \sim \delta t^{\alpha+1}$. An example trajectory of a ATTM model is shown in Fig. 1.6(a).

Continous time random walk (CTRW): This is a Brownian motion (with Gaussian distributed steps) with power-law distributed random waiting times between steps [54]. CTRW is a sub-diffusive or diffusive model that is not ergodic. An example trajectory of a CTRW model is shown in Fig. 1.6(b).

Fractional Brownian motion (FBM): This is a model with correlated Gaussian increments that are correlated [55]. Depending on the sign of the correlations, FBM can be either sub-diffusive (for negative correlations) or super-diffusive (for positive correlations). This model is ergodic. An example trajectory of a FBM model is shown in Fig. 1.6(c).

Lévy walks (LW): Lévy walk is a model where the particle is always travelling with a constant velocity in a random direction that randomly changes [56]. The duration of walks in each random direction is power-law distributed. Lévy walks are super-diffusive and non-ergodic. An example trajectory of a LW model is shown in Fig. 1.6(d).

Scaled Brownian motion (SBM): This is a model with deterministically changing diffusion coefficient, also known as time-rescaled Brownian motion [57]. SBM can simply be obtained by simulating a regular Brownian motion with rescaled time ($t \to t^{\alpha}$). An example trajectory of a SBM model is shown in Fig. 1.6(e).

There is a number of other models that undergo anomalous diffusion as well as due to the potential energy landscape [58]. For the purpose of this thesis, we will consider these models as well as active Brownian motion [48], which is also an anomalous diffusion and has been widely used to model artificial and natural microswimmers.

Active Brownian Motion

Lots of biological organisms can propel themselves in a liquid environment, such as *Escherichia coli* [59, 60]. This permits them to have a directed motion, although this is disturbed by the rotational diffusion or tumbling motion [61] in longer timescales. Whether they are smooth swimmers or run-and-tumble bacteria, they exhibit similar statistics [62]. Similar to biological swimmers, artificial microswimmers can also have directed motion by creating an asymmetry in their vicinity, either by chemical reactions [63–65], thermophoresis [66] or critical demixing [67]. Active Brownian motion can be described by the following

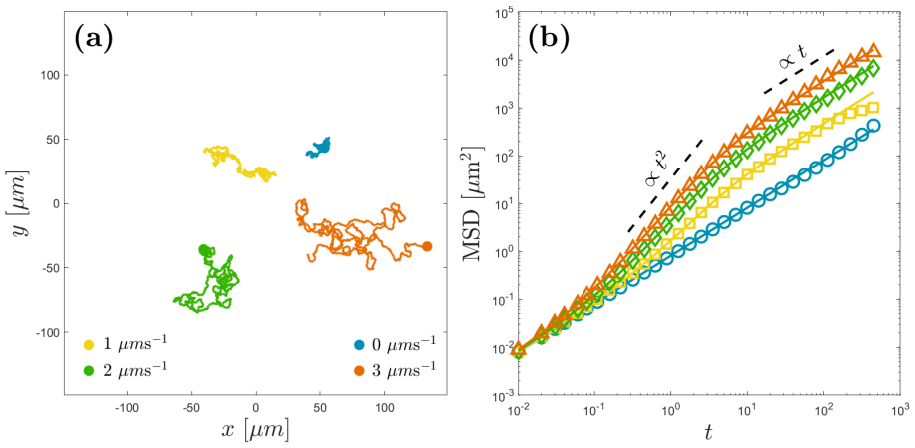

Figure 1.7: **Active Brownian motion and the mean square displacement (MSD) of active Brownian particles. (a)** Simulated active Brownian motion (Eq. 1.32, $D_T = 2 \times 10^{-13}$, $D_R = 0.5$) for swimming velocities of $V = 0$ (blue trajectory), $V = 1$ μm/s (yellow trajectory), $V = 2$ μm/s (green trajectory) and $V = 3$ μm/s (orange trajectory). **(b)** Corresponding mean square displacements of these microswimmers obtained by numerically simulating Eq. 1.32 (symbols) and the analytical solution (Eq. 1.35, lines).

equations of motion [65]:

$$\dot{x} = V\cos(\phi)\sqrt{2D_T}W_x(t) \tag{1.32}$$

$$\dot{y} = V\sin(\phi)\sqrt{2D_T}W_y(t) \tag{1.33}$$

$$\dot{\phi} = \sqrt{2D_R}W_\phi(t) \tag{1.34}$$

where ϕ represents the orientation of the self-propelled particle, which is subject to rotational diffusion (with rotational diffusion coefficient D_R) and V is the swimming velocity. Here, W_x, W_y and W_ϕ are white noises with mean zero and variance 1. I numerically demonstrate active Brownian motion for various velocities in Fig. 1.7(a). The mean square displacement of such a swimmer in 2 dimensions can be analytically derived as [65, 68]:

$$\mathrm{MSD}(t) = [4D_T + 2V^2\tau_R]t + 2V^2\tau_R^2\left[e^{-t/\tau_R} - 1\right] \tag{1.35}$$

while $\tau_R = D_R^{-1}$ represents the characteristic timescale of the particle's rotational motion. I numerically demonstrate Eq. 1.35 in Fig. 1.7(b) where

Both natural and artificial activity play a massive role advancing research in microbiology, nanotechnology and statistical physics [48]. When the active noise is present in the medium, lots of interesting out-of-equilibrium phenomena occur such as crowd control [69], directed transport [70–74], cluster formation [75–77] and energy harvesting from a single bath [78, 79]. I underline that none of these are possible to observe in a Markovian environment. Therefore, it is very compelling and important to understand to what extent the rules of

equilibrium and nonequilibrium thermodynamics will hold under the presense of non-Markovian (correlated) active noise. In **Paper I** [16], I show that an active system can behave like a thermal system that is held at a higher effective temperature if the length scales of the trapping potential is larger than the characteristic length of the active noise. I also demonstrate experimentally that if the particle is confined into a length scale that is smaller than this characteristic length, the system does not represent any equivalent thermal bath with an effective temperature. This can be shown from its steady state distribution behaviour as well as its response to nonequilibrium processes [16].

1.4 Analysis of stochastic trajectories

From single molecules to stock markets, many systems in physics and biology exhibit diffusion dynamics whose measurements yield stochastic trajectories. Examples include Brownian particles in a potential energy landscape, animals that search for food or changes in climate. Therefore, it is crucial to accurately analyze these trajectories and extract a greater amount of information that is contained within these noisy sequences. The type of analysis can be done to characterize the underlying dynamics [80], to predict future states [81] or to calibrate an experimental setup [82]. However, analyzing stochastic trajectories is challenging because often the experimentally obtained trajectories are limited in length [83, 84] and corrupted by measurement noise [85].

An important task that is performed via analysis of single trajectories is the measurement of force fields. Many experiments in biology, physics and material science requires an accurate measurement of the microscopic force fields [5, 86–88]. Examples include interparticle interactions [89–91], elasticity of cells [92, 93] and nonequilibrium relations [34, 38, 94, 95]. When the force field is widely known and the a large amount of data is available (such as an optically trapped particle in a harmonic potential), there are several methods to perform calibration such as the variance method, distribution method and power spectral density [5]. However, as the type of force field gets more arbitrary and the amount of data gets more limited, the number of existing methods that are applicable reduces dramatically. Only some of the methods, such as the distribution method, can be extended to more complicated force fields, but they still have to be conservative and the amount of data grows astronomically with the complexity of the potential. More advanced calibration methods, such as FORMA [82] can be employed for non-conservative fields, but it requires a high frequency measurement. **In Paper III** [96], I represent a data-driven approach for calibrating force fields that is powered by recurrent neural networks. I show that this method does not only overperform the existing methods but also expands possibilities of characterizing data in an arbitrary and even time dependent force fields that were not possible to predict before [96]. In addition, I made our method publicly accessible as a Python software package on Github that we name DeepCalib [97].

Another challenge in single trajectory analysis is the characterization of anomalous diffusion trajectories [80, 98]. Such an analysis can be done in different ways, such as classification of the underlying anomalous diffusion model, inference of the anomalous diffusion exponent or the segmentation of the

single trajectories with different characteristics. All of these tasks get extremely challenging when the trajectories are short and have measurement errors [84]. These difficulties motivated scientists to organize the Anomalous Diffusion Challenge (AnDi Challenge [98]), which aimed to benchmark state-of-the-art analysis techniques for analyzing single anomalous diffusion trajectories in classification, inference and segmentation. This challenge started in March 2020 with the announcement of the challenge as well as the software package for generating standardized data-sets [99]. In **Paper IV** [100], I show a method (that we name RANDI) based on a data-driven approach that won 4/9 categories of the AnDi challenge. In fact, our team was the only team that ranked in the top three in all tasks, which shows the versatility of the method. In addition, we show that RANDI performs better than all methods that participated in the AnDi challenge in 8/9 categories (We did not have enough time during the challenge to fully apply our method to higher dimensions, which we did later during the writing of the manuscript). RANDI is publicly available as a Python package, which can readily be downloaded and used for further studies [101].

CHAPTER 2

Research results

2.1 Thermodynamics of a bacterial heat bath

As discussed in the introduction section, whether an active bath can be considered as a thermal bath at a higher effective temperature is a key question in active matter. Although there are studies that indicate that the effective temperatures can be used for active systems [102], various experimental observations show that such a system coupled to an active bath shows out-of-equilibrium behaviour. In addition, whether the fluctuation theorems of the stochastic thermodynamics apply to the systems that are coupled to an active environment is unknown [48]. This motivated our research in **Paper I** [16], in which we seeked for answers to these questions.

In **Paper I** [16], we start by comparing the free diffusion trajectories of the particles that are coupled to a thermal bath and active bath. This allows us to characterize the motion of a Brownian particle in the active system. Experimentally, we recorded the trajectory of a Brownian particle that is in a thermal bath (blue trajectory, Fig 2.1(a)) and compared it to that of a particle placed in an active bath that. We realized the active bath by culturing motile *E. coli* bacteria [103]. We show that the trajectories in the active bath (orange trajectory, Fig 2.1(a)) yield persistent motion at shorter length (time) scales and diffusive behaviour at the longer length (time) scales. This is presented also in the mean squared displacement of the particle (right panel, Fig 2.1(a)) that transitions from super-diffusion at short length (time) scales to diffusion at long length (time) scales, in agreement with the previous studies [102, 103]. This is due to the active noise that is correlated at shorter length (time) scales, as presented in Eq. 1.35.

We also show that when a particle in an active bath is trapped in a harmonic potential that has longer length scales than the persistence length of the active bath, the system can be characterized with a higher effective temperature as the distribution is still Gaussian. However, if the particle is confined into smaller length scales than its characteristic persistence length, the distributions become non-Gaussian, which indicates that the system cannot be characterized with a higher effective temperature, as the distribution of a Brownian particle in a harmonic trap should always be Gaussian at all temperatures. As shown in Fig. 2.1(b), this becomes particularly evident when looking at the heavy tails of

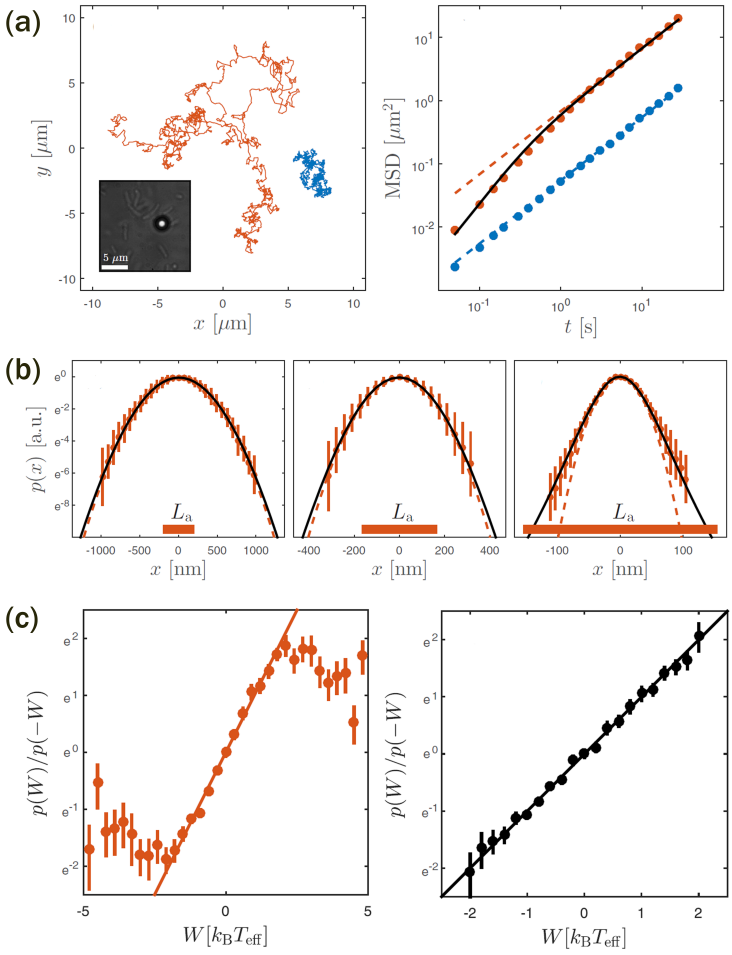

Figure 2.1: **Non-Boltzmann stationary distributions and nonequilibrium relations in an active bath. (a)** Unlike in water (blue trajectory, left panel), a Brownian particle ($R = 4.2$ μm) in an active bath has a persistent motion (orange trajectory, left panel) in short length (time) scales. This is also visible in the comparison of mean-square displacements (right panel). **(b)** When confined into larger scales than the persistence length (L_a,orange bar) in an active bath, a Brownian particle has a Gaussian distribution in a harmonic trap (left). However, the distribution becomes highly non-Gaussian as the particle is confined into smaller lengthscales than the persistence length (right). **(c)** The Crooks fluctuation theorem (solid line, left panel) does not work in active bath with an effective temperature approach, but it can be recovered with effective potentials that is derived from experimental stationary distributions (right panel) [16].

the distribution, when the particle is confined in a length scale that is shorter than its persistence length (orange bars, Fig. 2.1(b)) in the active bath.

Finally, we perform nonequilibrium measurements on the particle in an active bath by moving the trapping potential back and forth with a constant period. We demonstrate that the nonequilibrium relations, such as Crooks fluctuation theorem (left panel, Fig. 2.1(c)), Jarzynski equality and the integral fluctuation theorem, do not hold for particles that are coupled to active baths due to their non-Boltzmann behaviour at the stationary state. Nevertheless, we show that these relations can be recovered by using an effective potential energy that satisfies the Boltzmann distribution for the stationary state.

My contributions

The results in **Paper I** is a product of a fruitful collaboration of a number of authors (Ali-Reza Moradi, Erçağ Pince, Gökhan Barış Bağcı, Alberto Imparato and Giovanni Volpe) that worked in great harmony. I contributed to the initial discussions and designing of the experiments with Giovanni Volpe, building the experimental setup with Ali-Reza Moradi, performing all the experiments as well as analyzing data. Erçağ Pince provided help with the development of the bacterial solution. Gokhan Baris and Alberto Imparato provided theoretical support. I have made all the experimental measurements and data analysis that is presented in all figures. I have made the programming and operation of nonequilibrium experiments where we were required to change the trap position as a function of time. I interpreted the results with Gökhan Barış Bağcı, Alberto Imbarato and Giovanni Volpe. I designed and prepared all the figures and contributed to the preparation of the manuscript.

2.2 Experimental realization of a minimal heat engine

Microscopic heat engines are capable of harvesting energy and generate rotational motion in a microscopic environment. The first microscopic Stirling engine was realized by Blickle and Bechinger [29] and microscopic Carnot engine by Martinez et. al. [30]. Both are great examples of how energy can be harvested in microscopic environments with inspirations from the classical thermodynamics, by externally controlling the system parameters in a time cycle. In **Paper II** [31], we experimentally realized a Brownian gyrator that was initially proposed by Reimann [32]. The Brownian gyrator is not only operating between two heat baths as a heat engine autonomously in a controllable way, but also creates torque in a microscopic environment.

In **Paper II** [31], we realized a Brownian gyrator by experimentally creating an elliptical potential (along x' and y', Fig. 2.2(a)) and coupled to two perpendicular heat baths (along x and y, Fig. 2.2(a)) that have different temperatures. The elliptical potential was created by highly focusing an asymmetric laser beam by using a spatial light modulator [31]. The temperature asymmetry is created by increasing the effective temperature along one axis by adding artificial random forces that mimic thermal noise [104]. If the axes for the temperature and for the elliptical trap are not aligned, the asymmetry that is created results in a systematic rotational motion. This motion is shown as

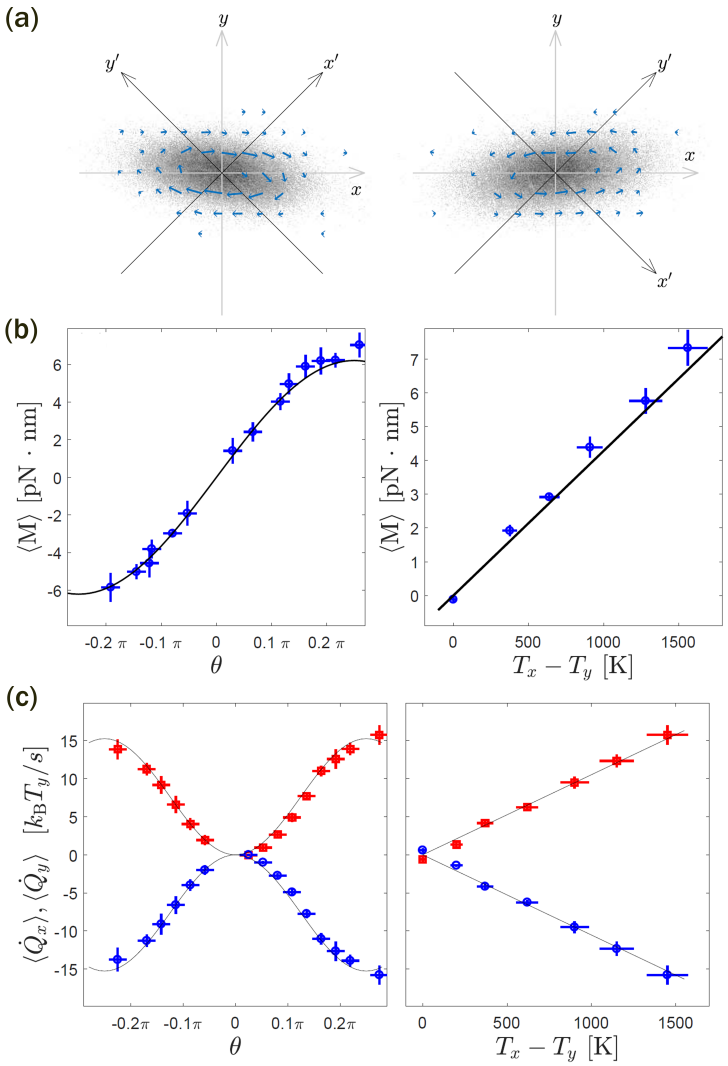

Figure 2.2: **Realization of a minimal microscopic heat engine.** **(a)** Position distribution of a Brownian particle that is placed in an elliptical trap ($k_{x'} = 1.63$ pN/μm and $k_{x'} = 0.86$ pN/μm) in an environment with different effective temperatures ($T_x = 1750$ K and $T_y = 292$ K). The blue arrows represent the drift fields of that are obtained from the particle trajectory. The direction of the flow this drift can be controlled by the alignment of the elliptical potential. **(b)** Measured torque as a function of the relative orientation of the temperature anisotropy and those of the potential (left panel). The torque as a function of the difference in temperature is shown in the right panel. **(c)** The heat exchange as a function of the relative orientation of the temperature anisotropy and those of the potential (left panel). The torque as a function of the difference in temperature is shown in the right panel. The symbols represent the experimental data and the solid lines are the theoretical predictions [31].

the experimentally measured torque values in Fig. 2.2(b). These measurements show great agreement with theoretical predictions. Importantly, we show that the rotation and the amplitude of this torque can be controlled by changing the angle between x and x' or by changing the difference in effective temperatures along x and y, as shown in Fig. 2.2(b).

In addition, we also derive the expression for the heat exchange between the two heat baths as a function of both the alignment of the elliptical trap and the difference in effective temperatures along x and y. We show excellent agreement between our theoretical predictions and the experimental results, as shown in Fig. 2.2(c). It is important to underline that, unlike torque, the direction of the heat flow cannot be controlled with the alignment of the elliptical trap, at it is thermodynamically impossible. Nevertheless, we can control the quantity of heat flow between the two heat baths by tuning the alignment of the elliptical trap or the difference in effective temperatures along x and y.

My contributions

The experiments that were performed in **Paper II** was proposed by Lennart Dabelow, Stefano Bo and Ralf Eichhorn, who also provided theoretical support. I made the initial numerical simulations and concluded with Giovanni Volpe that this is a promising and experimentally feasible project. I built the experimental setup and performed measurements together with Jalpa Soni. I have analyzed the data and and prepared the figures of the manuscript. Giuseppe Pesce provided support with the synthetic random forces that increased the effective temperature. I also contributed to the preparation of the manuscript.

2.3 Calibration of force fields

Around the half time of my Ph.D., we started getting interested in deep learning and its applications to microscopic systems. After developing a particle tracking software [105], we discussed on a new method to calculate force fields from Brownian trajectories. Calibration of force fields has been a challenge, especially from trajectories that are limited in length [82, 106, 107]. This analysis gets particularly difficult if the underlying force field is non-conservative or time varying. In **Paper III** [96], we present a machine learning based method to calculate force fields directly from individual trajectories that can be applied to any force field system including non-conservative or time-varying force fields. We name our method DeepCalib that we publish as a free Python software package for anyone who would need to use it [97].

Unlike algorithmic methods, DeepCalib is a data-driven method to analyze Brownian trajectories in order to predict the underlying force field. We used recurrent neural networks, in particular long-short-term-memory (LSTM) layers. We train the network using simulated data. A schematic view of DeepCalib is shown in Fig. 2.3(a). For the case of harmonic trap, all of the methods including the variance method, autocorrelation method and FORMA show systematically inaccurate results, particularly, if the stiffness is too small or too large. However, DeepCalib provides the best results through a wide range of stiffness values. It is important to underline that these results that we present are for the ideal

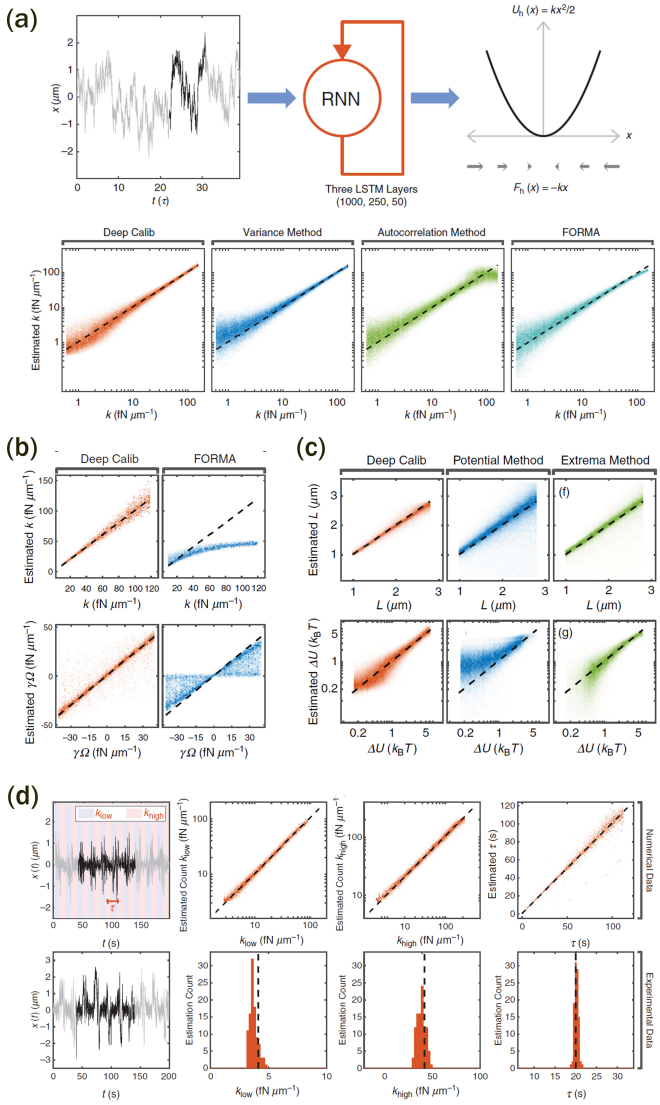

Figure 2.3: **Calibration of microscopic force fields using machine learning (a)** The trajectory of a Brownian particle in a harmonic trap is given as an input to the recurrent neural network (RNN) to predict the stiffness parameter of the trap (k). The bottom panel shows comparisons of the predictions from various methods. As it can be seen, DeepCalib provides the most accurate results through the entire range. **(b)** Calibration of a rotational force field using DeepCalib (orange density plots) outperforms FORMA (blue density plots). **(c)** Calibration of a double well potential using DeepCalib (orange density plots) outperforms the potential method (blue density plots) and the extrema method (green density plots). **(d)** Calibration of a dynamical nonequilibrium force field when the stiffness of a harmonic trap is oscillating between k_{low} and k_{high} with a period τ. There are no existing calibration methods for such a force field that is time-varying. Evidently, DeepCalib successfully predicts all parameters both for simulated (top panel) and experimental (bottom panel) trajectories. [96]

conditions with simulated data that has no artifacts. We also demonstrate in **Paper III** [96] that DeepCalib is robust against measurement noise, varying viscosity, asymmetries in force fields and varying input length.

We also show that DeepCalib can accurately calculate non-conservative rotational force fields better than the existing methods, where we have two parameters that represent the force field, the central force stiffness k and the rotational parameter Ω. Although being accurate for lower values of the k, FORMA struggles at higher force values because of the data points becoming uncorrelated. DeepCalib is able to estimate the parameters of the rotational force field better than FORMA as shown in Fig. 2.3(b).

DeepCalib improves also the calibration of a double-well over the existing methods, where we have a potential energy profile with two wells of depth ΔU, separated by a distance L. We demonstrate that DeepCalib provides more accurate results than the standard methods as shown in Fig. 2.3(c). We also demonstrate in **Paper III** [96] that in fact Deepcalib is robust in analyzing experimental data that has a slightly different potential energy profile than the simulations. We also show that DeepCalib can be extended to asymmetric double wells.

Finally, we show that DeepCalib can be used to calibrate dynamical nonequilibrium force fields that vary over time. It is important to point out that no calibration methods exist for such force fields. As an example of an arbitrarily time-varying force field, we choose a harmonic trap with changing stiffness between k_{low} and k_{high} with a period τ. As it can be shown in the top panel of Fig. 2.3(d), DeepCalib can very accurately predict all of these three parameters from a short trajectory of 1000 data points. We also show that DeepCalib can also be applied to experimental data that has the same protocol (bottom panel, Fig. 2.3(d)).

All of the results we present in **Paper III** [96] can be reproduced by using the example files that are publicly available on Github [97].

My contributions

I developed the method DeepCalib and tested on numerical data. Tobias Thalheim and Frank Cichos provided the experimental data for testing the robustness of DeepCalib. I prepared the codes and the example files of the software that is published on Github [97], I received feedback from all coauthors on the example code files. I prepared all the figures as well as the supplementary material. I and Stefano Bo drafted the manuscript that was revised by all coauthors.

2.4 Characterizing of anomalous diffusion trajectories

During the period when we were developing DeepCalib [96], a competition for characterizing anomalous diffusion trajectories (named AnDi Challenge) was announced. I decided to compete in this competition with my collaborator Stefano Bo. We used a similar neural network architecture to the one of

DeepCalib as we found it powerful to analyse stochastic trajectories. We developed a workflow for all tasks in the ANDI challenge including classification, inference and segmentation of the anomalous diffusion trajectories that we explain in **Paper IV** [100]. Our method was ranked first in the 4/9 categories of the challenge and top three in all of the categories, which proves the versatility and power of our method that we name RANDI. We also published RANDI as a free Python software package [101].

RANDI uses machine learning to characterize anomalous diffusion trajectories. Specifically, we used a recurrent neural network architecture (Fig. 2.4(a)) with two LSTM layers. The data required for training is obtained by simulating trajectories using ANDI datasets package [99, 108]. We found out that the performance of each neural network is better when they are trained for inputs that are length specific, as shown in Fig. 2.4(b). For this reason, we trained multiple neural networks in order to analyze trajectories of random length that has uniform distribution between 10 and 1000. In the classification task, the neural network receives a short input trajectory (with an unknown random exponent) that is corrupted with measurement noise and outputs the probability of the input belonging to one of the anomalous diffusion models (ATTM, CTRW, FBM, LW, SBM, see Section 1.3). We used multiple networks for different lengths of input trajectories. With this method RANDI manages to classify trajectories with an overall accuracy of 87.05% for 1D, 89.16% for 2D and 93.76% for 3D trajectories, all of them are better than the best results that are submitted to the ANDI challenge, which shows that our method stands out in classifying the anomalous diffusion trajectories [100]. The accuracy of RANDI as a function of input length for all dimensions is shown in Fig. 2.4(b).

RANDI is also capable of inferring the anomalous diffusion exponent α (MSD = t^{α}) of the trajectories. For this task, we used a similar RNN architecture to the one used for classification. The RNN has only one output node that is connected directly to the 2 LSTM layers. For inference of the anomalous diffusion exponent, RANDI has a mean absolute error of 0.1558 for 1D trajectories, which is only 2.4% higher than the best results that are submitted to the ANDI challenge. In higher dimensions RANDI has a mean absolute error of 0.1345 for 2D and 0.1109 for 3D, which are better than the best results that are submitted to the ANDI challenge [100]. The details of the accuracies of all dimensions as a function of the input trajectory length is shown in Fig. 2.4(c).

Finally, RANDI is also able to perform segmentation of anomalous diffusion trajectories with the state-of-the-art accuracy. This task includes a switching time of the anomalous diffusion model and/or the anomalous diffusion exponent at a random time in a trajectory. An example input trajectory is shown in Fig. 2.4(d), where we predict the model class for both the first and the second segment, the switching time t_s as well as the anomalous diffusion exponent of both segments. Again, with the segmentation task, RANDI's segmentation is better than the best results that are submitted to the ANDI challenge [100].

The training and the analysis we perform with RANDI can be repeated by running the example codes on the Github page of RANDI [101].

My contributions

Paper IV [100] is a great result of a very fruitful collaboration with Stefano Bo. I and Stefano Bo weekly discussed the models, training results and the output accuracies our method provided during and after the ANDI challenge in order to push it to the limit where we did not only think about which method would provide the most accurate results but also thoroughly investigated all possible ways of improvement such as pre-processing of the data, normalization, fine tuning the hyper-parameters and reshaping input. I contributed to the discussion and development of the methodology that we followed during the ANDI challenge. I built the software for training networks together with Stefano. I prepared the data-sets and performed the training of the networks, analyzed the results, prepared the figures and contributed to the drafting of the manuscript.

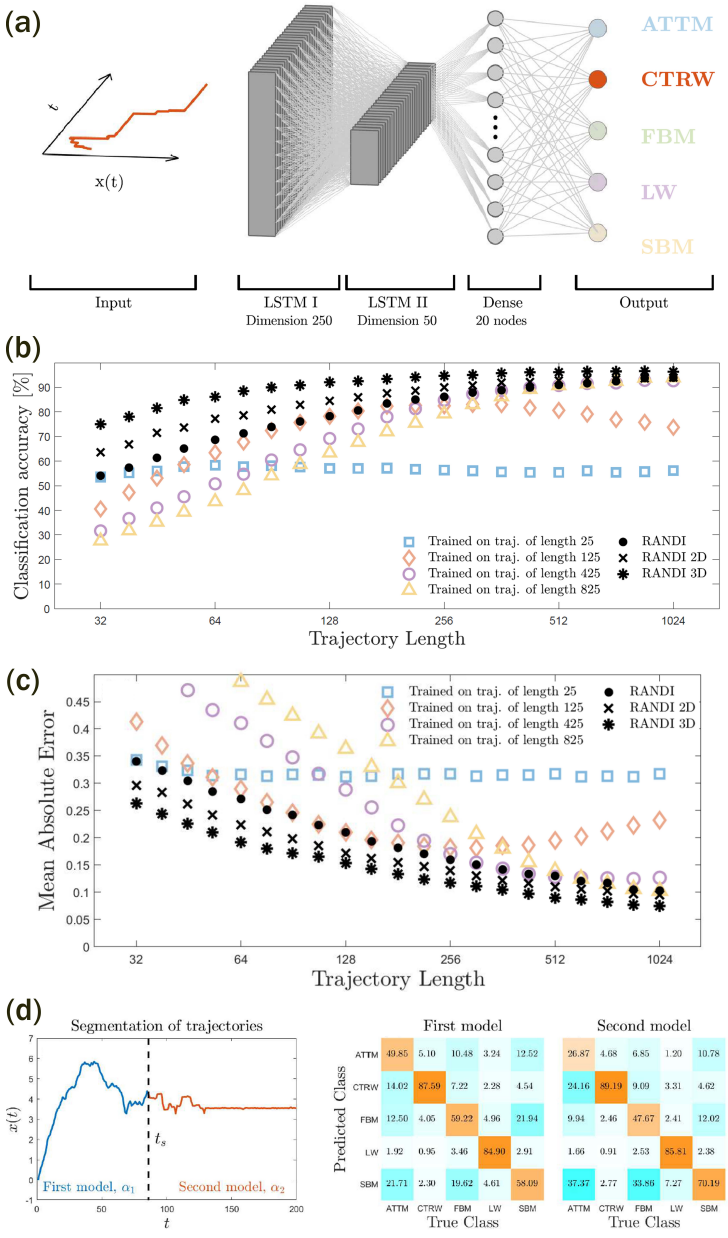

Figure 2.4: **Classification, inference and segmentation of anomalous diffusion trajectories using machine learning (a)** The architecture of the recurrent neural network (RNN) we use to analyse anomalous diffusion trajectories. **(b)** The accuracy of RANDI in classifying the anomalous diffusion trajectories that is better than the best results submitted to anomalous diffusion challenge in all dimensions. **(c)** The accuracy of RANDI in inferring the anomalous diffusion exponent. The results in 2D and 3D are better than the best results submitted to anomalous diffusion challenge. **(d)** The accuracy of RANDI in segmenting the anomalous diffusion trajectories. RANDI provides more accurate results than the best results submitted to the anomalous diffusion challenge in all dimensions. [100]

CHAPTER 3

Conclusions and outlook

During the last few years, advances in research on anomalous diffusion, active matter and deep learning has been growing very rapidly. During my Ph.D. studies, I felt challenged by the pace of progress in these fields, but enjoyed working on all of these interesting subjects, which are crucial to understand and interpret the dynamics of the microscopic world.

In **Paper I** [16], I showed under which conditions the statistics of an active bath can be characterized with an effective temperature. Although there had been both studies where the use of effective temperature is useful [102, 103] and where it is not convenient [69, 70, 78], I showed a transition that highlights the importance of the length scales of the confinement. I also showed that the nonequilibrium relations do not hold for particles that are coupled to an active bath. Nevertheless, I showed that they can be recovered by using an effective potential energy that ensures the Boltzmann distribution is satisfied. In particular, the work and heat values in an active matter system can be redefined using this effective potential. These results imply that the trajectories of a particle in an active bath yield entropy production [109–112]. As many systems including biological media are intrinsically active, the findings of **Paper I** [16] contributes to the possibility of applying nonequilibrium relations on systems that are coupled to active baths. The results of **Paper I** [16] played an important role in motivating further theoretical study of modelling the motion of a Brownian particle in an active bath [113–117].

Microscopic heat engines are promising tools to convert energy flows between heat reservoirs into work or useful motion in a microscopic environment. The first realizations of microscopic heat engines were based on externally driven protocols [29, 30, 118]. In **Paper II** [31], I experimentally realized a minimal microscopic heat engine that is autonomous. This is realized by creating an elliptical confinement and different temperatures along two dimensions. When the principle axes of the elliptical trap and the temperature anisotropy are not aligned, the system symmetry is broken. This creates a torque that is acting on the Brownian particle. We show that the quantity and the direction of this torque can be controlled by tuning the alignment of the elliptical trap and the temperature asymmetry. An important advantage of the Brownian gyrator is that it directly transfers the heat flow into rotational motion in the microscopic environment [31]. This experiment features an autonomous yet controllable

microscopic heat engine with minimal degree of complexity.

The interpretation of most experiments in microscopic thermodynamics (such as the ones the ones I present in **Paper I** [16] and **Paper II** [31]), biophysics and soft matter depend on the initial calibration of the force fields that are used in the experimental protocol. Therefore, it is fundamental to calibrate the force fields accurately in order to extract the most reliable information the experimental trajectories. In **Paper III** [96], I present a data-driven method to calibrate the force fields from Brownian trajectories that outperforms the standard methods. Importantly, this method is made available as a free Python software package, named DeepCalib [97] that users can customize and apply to their systems. DeepCalib is capable of accurately estimating the parameters of any force field that is non-conservative or time-varying. I also present in the **Paper III** [96] that Deepcalib works perfectly on experimental data and it is robust against measurement noise, varying viscosity and varying input length. Finally, DeepCalib makes it possible to calibrate complex dynamical force fields that no standard calibration methods exist. It can be used to improve the accuracy of calibration for microscopic heat engines, to analyze trajectories that are in a complex force field and to extract more information from experimental trajectories with limited length.

As **Paper III** [96] shows, the machine learning based methods perform very well in analysing stochastic trajectories. Neural networks become particularly useful in analysing anomalous diffusion trajectories as the existing methods for characterizing anomalous diffusion is limited [80, 85]. Therefore, I have developed a software for classification, inference and segmentation of anomalous diffusion trajectories that provides better results than all methods participating in the AnDi challenge [108] in in 8 tasks out of 9. This software is presented in **Paper IV** [100] is named RANDI and it is available as a free Python software package [101]. **Paper IV** [100] presents that RANDI performs better than all the methods that are competed in the AnDi challenge in classification and segmentation of the anomalous diffusion trajectories in all dimensions. For the inference of the anomalous diffusion trajectories, RANDI provides results better than the best result submitted to the AnDi challenge in 2D and 3D. Together with **Paper III** [96], **Paper IV** [100] shows that recurrent neural networks are very powerful and versatile for analysis of short stohastic trajectories.

During my Ph.D., I have carried out research in a variety of subjects including active matter, optical trapping, microscopic thermodynamics, anomalous diffusion and deep learning. This has allowed me to learn theoretical knowledge, performing simulations, building experimental setups, making measurements and analyzing data. Every project that I have been involved in was genuinely interesting that made my challenging journey enjoyable. It was absolutely pleasant to work with such a wide range of subjects, from stochastic thermodynamics to deep learning applications in microscopy. Most importantly, I have learned how to navigate through the ocean of scientific knowledge and find the right drops that is useful for me to solve my problems.

Bibliography

1. Langevin, P. CR Acad. Sci.(Paris) 146, 530; trans. Lemons, DS & Gythiel, A.(1997). *Am. J. Phys* vol. 65, 1079–1081 (1908).
2. Einstein, A. Un the movement of small particles suspended in statiunary liquids required by the molecular-kinetic theory 0f heat. *Ann. Phys* vol. 17, 549–560 (1905).
3. Volpe, G. & Volpe, G. Simulation of a Brownian particle in an optical trap. *American Journal of Physics* vol. 81, 224–230 (2013).
4. Ashkin, A., Dziedzic, J., Bjorkholm, J. & Chu, S. Observation of a single-beam gradient force optical trap for dielectric particles. *Optics letters* vol. 11, 288–290 (1986).
5. Jones, P., Maragó, O. & Volpe, G. *Optical tweezers: Principles and applications* (Cambridge University Press, 2015).
6. Ashkin, A., Dziedzic, J. M. & Yamane, T. Optical trapping and manipulation of single cells using infrared laser beams. *Nature* vol. 330, 769–771 (1987).
7. Ashkin, A. & Dziedzic, J. M. Optical trapping and manipulation of viruses and bacteria. *Science* vol. 235, 1517–1520 (1987).
8. Ashkin, A. Trapping of atoms by resonance radiation pressure. *Physical Review Letters* vol. 40, 729 (1978).
9. Maragò, O. M., Jones, P. H., Gucciardi, P. G., Volpe, G. & Ferrari, A. C. Optical trapping and manipulation of nanostructures. *Nature nanotechnology* vol. 8, 807 (2013).
10. Ashkin, A., Mourou, G. & Strickland, D. The 2018 Nobel Prize in physics: a gripping and extremely exciting tale of light. *Curr. Sci* vol. 115, 18441848 (2018).
11. Seifert, U. Stochastic thermodynamics, fluctuation theorems and molecular machines. *Reports on Progress in Physics* vol. 75, 126001 (2012).
12. Purcell, E. M. Life at low Reynolds number. *Am. J. Phys* vol. 45, 3–11 (1977).
13. Øksendal, B. in *Stochastic differential equations* 65–84 (Springer, 2003).
14. Platen, E. An introduction to numerical methods for stochastic differential equations. *Acta numerica* vol. 8, 197–246 (1999).

15. Shiryayev, A. in *Selected works of AN Kolmogorov* 62–108 (Springer, 1992).

16. Argun, A. *et al.* Non-Boltzmann stationary distributions and nonequilibrium relations in active baths. *Physical Review E* vol. 94, 062150 (2016).

17. Huang, K. Statistical mechanics. *New York—London* (1963).

18. Sekimoto, K. *Stochastic energetics* (Springer, 2010).

19. Martınez, I. A., Roldán, É., Dinis, L., Petrov, D. & Rica, R. A. Adiabatic processes realized with a trapped Brownian particle. *Physical review letters* vol. 114, 120601 (2015).

20. Sekimoto, K. Langevin equation and thermodynamics. *Progress of Theoretical Physics Supplement* vol. 130, 17–27 (1998).

21. Evans, D. J., Cohen, E. & Morriss, G. Probability of second law violations in shearing steady states. *Physical Review Letters* vol. 71, 2401 (1993).

22. Gallavotti, G. & Cohen, E. Dynamical ensembles in nonequilibrium statistical mechanics. *Physical Review Letters* vol. 74, 2694 (1995).

23. Evans, D. J. & Searles, D. J. Equilibrium microstates which generate second law violating steady states. *Physical Review E* vol. 50, 1645 (1994).

24. Lebowitz, J. L. & Spohn, H. A Gallavotti–Cohen-type symmetry in the large deviation functional for stochastic dynamics. *Journal of Statistical Physics* vol. 95, 333–365 (1999).

25. Kurchan, J. Fluctuation theorem for stochastic dynamics. *Journal of Physics A: Mathematical and General* vol. 31, 3719 (1998).

26. Carnot, S. Reflections on the motive power of fire, and on machines fitted to develop that power. *Paris: Bachelier* (1824).

27. Hänggi, P. & Marchesoni, F. Artificial Brownian motors: Controlling transport on the nanoscale. *Reviews of Modern Physics* vol. 81, 387 (2009).

28. Schmiedl, T. & Seifert, U. Efficiency at maximum power: An analytically solvable model for stochastic heat engines. *EPL (Europhysics Letters)* vol. 81, 20003 (2007).

29. Blickle, V. & Bechinger, C. Realization of a micrometre-sized stochastic heat engine. *Nature Physics* vol. 8, 143–146 (2012).

30. Martınez, I. A. *et al.* Brownian carnot engine. *Nature Physics* vol. 12, 67–70 (2016).

31. Argun, A. *et al.* Experimental realization of a minimal microscopic heat engine. *Physical Review E* vol. 96, 052106 (2017).

32. Filliger, R. & Reimann, P. Brownian gyrator: A minimal heat engine on the nanoscale. *Physical review letters* vol. 99, 230602 (2007).

33. Crooks, G. E. Entropy production fluctuation theorem and the nonequilibrium work relation for free energy differences. *Physical Review E* vol. 60, 2721 (1999).

34. Collin, D. *et al.* Verification of the Crooks fluctuation theorem and recovery of RNA folding free energies. *Nature* vol. 437, 231–234 (2005).

35. Gupta, A. N. *et al.* Experimental validation of free-energy-landscape reconstruction from non-equilibrium single-molecule force spectroscopy measurements. *Nature Physics* vol. 7, 631–634 (2011).

36. Jarzynski, C. Nonequilibrium equality for free energy differences. *Physical Review Letters* vol. 78, 2690 (1997).

37. Jarzynski, C. Equalities and inequalities: irreversibility and the second law of thermodynamics at the nanoscale. *Annu. Rev. Condens. Matter Phys.* vol. 2, 329–351 (2011).

38. Liphardt, J., Dumont, S., Smith, S. B., Jr., I. T. & Bustamante, C. Equilibrium information from nonequilibrium measurements in an experimental test of Jarzynski's equality. *Science* vol. 296, 1832–1835 (2002).

39. Harris, N. C., Song, Y. & Kiang, C.-H. Experimental free energy surface reconstruction from single-molecule force spectroscopy using Jarzynski's equality. *Physical review letters* vol. 99, 068101 (2007).

40. Schuler, S., Speck, T., Tietz, C., Wrachtrup, J. & Seifert, U. Experimental test of the fluctuation theorem for a driven two-level system with time-dependent rates. *Physical review letters* vol. 94, 180602 (2005).

41. An, S. *et al.* Experimental test of the quantum Jarzynski equality with a trapped-ion system. *Nature Physics* vol. 11, 193–199 (2015).

42. Berkovich, R., Klafter, J. & Urbakh, M. Analyzing friction forces with the Jarzynski equality. *Journal of Physics: Condensed Matter* vol. 20, 354008 (2008).

43. Saira, O.-P. *et al.* Test of the Jarzynski and Crooks fluctuation relations in an electronic system. *Physical review letters* vol. 109, 180601 (2012).

44. Klafter, J. & Sokolov, I. M. Anomalous diffusion spreads its wings. *Physics world* vol. 18, 29 (2005).

45. Barkai, E., Garini, Y. & Metzler, R. Strange kinetics of single molecules in living cells. *Phys. Today* vol. 65, 29–35 (2012).

46. Höfling, F. & Franosch, T. Anomalous transport in the crowded world of biological cells. *Reports on Progress in Physics* vol. 76, 046602 (2013).

47. Metzler, R., Jeon, J.-H., Cherstvy, A. G. & Barkai, E. Anomalous diffusion models and their properties: non-stationarity, non-ergodicity, and ageing at the centenary of single particle tracking. *Physical Chemistry Chemical Physics* vol. 16, 24128–24164 (2014).

48. Bechinger, C. *et al.* Active Brownian particles in complex and crowded environments. *arXiv preprint arXiv:1602.00081* (2016).

49. Ramaswamy, S. The mechanics and statistics of active matter. *Annual Review of Condensed Matter Physics* vol. 1, 323–345 (2010).

50. Erdmann, U., Ebeling, W., Schimansky-Geier, L. & Schweitzer, F. Brownian particles far from equilibrium. *The European Physical Journal B-Condensed Matter and Complex Systems* vol. 15, 105–113 (2000).

51. Hauser, M. & Schimansky-Geier, L. Statistical physics of self-propelled particles. *The European Physical Journal Special Topics* vol. 224, 1147–1150 (2015).

52. Schweitzer, F. & Farmer, J. D. *Brownian agents and active particles: collective dynamics in the natural and social sciences* (Springer Science & Business Media, 2007).

53. Massignan, P. *et al.* Nonergodic subdiffusion from Brownian motion in an inhomogeneous medium. *Physical review letters* vol. 112, 150603 (2014).

54. Scher, H. & Montroll, E. W. Anomalous transit-time dispersion in amorphous solids. *Physical Review B* vol. 12, 2455 (1975).

55. Mandelbrot, B. B. & Van Ness, J. W. Fractional Brownian motions, fractional noises and applications. *SIAM review* vol. 10, 422–437 (1968).

56. Klafter, J. & Zumofen, G. Lévy statistics in a Hamiltonian system. *Physical Review E* vol. 49, 4873 (1994).

57. Lim, S. & Muniandy, S. Self-similar Gaussian processes for modeling anomalous diffusion. *Physical Review E* vol. 66, 021114 (2002).

58. Volpe, G., Volpe, G. & Gigan, S. Brownian motion in a speckle light field: tunable anomalous diffusion and selective optical manipulation. *Scientific reports* vol. 4, 1–6 (2014).

59. Berg, H. C. *E. coli in Motion* (Springer Science & Business Media, 2008).

60. Romanczuk, P., Bär, M., Ebeling, W., Lindner, B. & Schimansky-Geier, L. Active brownian particles. *The European Physical Journal Special Topics* vol. 202, 1–162 (2012).

61. Tailleur, J. & Cates, M. Statistical mechanics of interacting run-and-tumble bacteria. *Physical review letters* vol. 100, 218103 (2008).

62. Cates, M. & Tailleur, J. When are active Brownian particles and run-and-tumble particles equivalent? Consequences for motility-induced phase separation. *EPL (Europhysics Letters)* vol. 101, 20010 (2013).

63. Ismagilov, R. F., Schwartz, A., Bowden, N. & Whitesides, G. M. Autonomous Movement and Self-Assembly. *Angewandte Chemie International Edition* vol. 41, 652–654 (2002).

64. Paxton, W. F. *et al.* Catalytic nanomotors: autonomous movement of striped nanorods. *Journal of the American Chemical Society* vol. 126, 13424–13431 (2004).

65. Howse, J. R. *et al.* Self-motile colloidal particles: from directed propulsion to random walk. *Physical review letters* vol. 99, 048102 (2007).

66. Jiang, H.-R., Yoshinaga, N. & Sano, M. Active motion of a Janus particle by self-thermophoresis in a defocused laser beam. *Physical review letters* vol. 105, 268302 (2010).

67. Buttinoni, I., Volpe, G., Kümmel, F., Volpe, G. & Bechinger, C. Active Brownian motion tunable by light. *Journal of Physics: Condensed Matter* vol. 24, 284129 (2012).

68. Uhlenbeck, G. E. & Ornstein, L. S. On the theory of the Brownian motion. *Physical review* vol. 36, 823 (1930).

69. Pinçe, E. *et al.* Disorder-mediated crowd control in an active matter system. *Nature communications* vol. 7 (2016).

70. Koumakis, N., Maggi, C. & Di Leonardo, R. Directed transport of active particles over asymmetric energy barriers. *Soft matter* vol. 10, 5695–5701 (2014).

71. Koumakis, N., Lepore, A., Maggi, C. & Di Leonardo, R. Targeted delivery of colloids by swimming bacteria. *Nature communications* vol. 4 (2013).

72. Volpe, G., Buttinoni, I., Vogt, D., Kümmerer, H.-J. & Bechinger, C. Microswimmers in patterned environments. *Soft Matter* vol. 7, 8810–8815 (2011).

73. Kaiser, A., Wensink, H. & Löwen, H. How to capture active particles. *Physical review letters* vol. 108, 268307 (2012).

74. Galajda, P., Keymer, J., Chaikin, P. & Austin, R. A wall of funnels concentrates swimming bacteria. *Journal of bacteriology* vol. 189, 8704–8707 (2007).

75. Cates, M. E. & Tailleur, J. Motility-induced phase separation. *arXiv preprint arXiv:1406.3533* (2014).

76. Suma, A., Gonnella, G., Marenduzzo, D. & Orlandini, E. Motility-induced phase separation in an active dumbbell fluid. *EPL (Europhysics Letters)* vol. 108, 56004 (2014).

77. Reichhardt, C. & Reichhardt, C. J. O. Absorbing phase transitions and dynamic freezing in running active matter systems. *Soft matter* vol. 10, 7502–7510 (2014).

78. Di Leonardo, R. *et al.* Bacterial ratchet motors. *Proceedings of the National Academy of Sciences* vol. 107, 9541–9545 (2010).

79. Maggi, C. *et al.* Self-Assembly of Micromachining Systems Powered by Janus Micromotors. *Small* vol. 12, 446–451 (2016).

80. Bo, S., Schmidt, F., Eichhorn, R. & Volpe, G. Measurement of anomalous diffusion using recurrent neural networks. *Physical Review E* vol. 100, 010102 (2019).

81. Zhang, L., She, Q. & Guo, P. Stochastic trajectory prediction with social graph network. *arXiv preprint arXiv:1907.10233* (2019).

82. Garcıa, L. P., Pérez, J. D., Volpe, G., Arzola, A. V. & Volpe, G. High-performance reconstruction of microscopic force fields from Brownian trajectories. *Nature communications* vol. 9, 1–9 (2018).

83. Meroz, Y. & Sokolov, I. M. A toolbox for determining subdiffusive mechanisms. *Physics Reports* vol. 573, 1–29 (2015).

84. Weron, A., Janczura, J., Boryczka, E., Sungkaworn, T. & Calebiro, D. Statistical testing approach for fractional anomalous diffusion classification. *Physical Review E* vol. 99, 042149 (2019).

85. Burnecki, K., Kepten, E., Garini, Y., Sikora, G. & Weron, A. Estimating the anomalous diffusion exponent for single particle tracking data with measurement errors-An alternative approach. *Scientific reports* vol. 5, 1–11 (2015).

86. Wu, M. C. Optoelectronic tweezers. *Nature Photonics* vol. 5, 322–324 (2011).

87. Braun, M. & Cichos, F. Optically controlled thermophoretic trapping of single nano-objects. *ACS nano* vol. 7, 11200–11208 (2013).

88. Gieseler, J. *et al.* Optical tweezers: A comprehensive tutorial from calibration to applications. *arXiv preprint arXiv:2004.05246* (2020).

89. Su, K.-H. *et al.* Interparticle coupling effects on plasmon resonances of nanogold particles. *Nano letters* vol. 3, 1087–1090 (2003).

90. Yada, M., Yamamoto, J. & Yokoyama, H. Direct observation of anisotropic interparticle forces in nematic colloids with optical tweezers. *Physical review letters* vol. 92, 185501 (2004).

91. Paladugu, S. *et al.* Nonadditivity of critical Casimir forces. *Nature communications* vol. 7, 1–8 (2016).

92. Mills, J., Qie, L., Dao, M., Lim, C. & Suresh, S. Nonlinear elastic and viscoelastic deformation of the human red blood cell with optical tweezers. *Molecular & Cellular Biomechanics* vol. 1, 169 (2004).

93. Sleep, J., Wilson, D., Simmons, R. & Gratzer, W. Elasticity of the red cell membrane and its relation to hemolytic disorders: an optical tweezers study. *Biophysical journal* vol. 77, 3085–3095 (1999).

94. Jun, Y., Gavrilov, M. & Bechhoefer, J. High-precision test of Landauer's principle in a feedback trap. *Physical review letters* vol. 113, 190601 (2014).

95. Bérut, A. *et al.* Experimental verification of Landauer's principle linking information and thermodynamics. *Nature* vol. 483, 187–189 (2012).

96. Argun, A., Thalheim, T., Bo, S., Cichos, F. & Volpe, G. Enhanced force-field calibration via machine learning. *Applied Physics Reviews* vol. 7, 041404 (2020).

97. Argun, A., Thalheim, T., Bo, S., Cichos, F. & Volpe, G. *DeepCalib* http://github.com/softmatterlab/DeepCalib. Version 1.0. 2020.

98. Munoz-Gil, G., Garcia-March, M. A., Manzo, C., Martın-Guerrero, J. D. & Lewenstein, M. Single trajectory characterization via machine learning. *New Journal of Physics* vol. 22, 013010 (2020).

99. Muñoz-Gil, G. *et al.* The Anomalous Diffusion Challenge dataset (Mar. 2020).

100. Argun, A., Volpe, G. & Bo, S. Classification, inference and segmentation of anomalous diffusion with recurrent neural networks. *arXiv preprint arXiv:2104.00553* (2021).

101. Argun, A., Volpe, G. & Bo, S. *RANDI*

102. Maggi, C. *et al.* Generalized energy equipartition in harmonic oscillators driven by active baths. *Phys. Rev. Lett.* vol. 113, 238303 (2014).

103. Wu, X.-L. & Libchaber, A. Particle diffusion in a quasi-two-dimensional bacterial bath. *Physical Review Letters* vol. 84, 3017 (2000).

104. Martinez, I. A., Roldán, E., Parrondo, J. M. & Petrov, D. Effective heating to several thousand kelvins of an optically trapped sphere in a liquid. *Physical Review E* vol. 87, 032159 (2013).

105. Helgadottir, S., Argun, A. & Volpe, G. Digital video microscopy enhanced by deep learning. *Optica* vol. 6, 506–513 (2019).

106. Wu, P., Huang, R., Tischer, C., Jonas, A. & Florin, E.-L. Direct measurement of the nonconservative force field generated by optical tweezers. *Physical review letters* vol. 103, 108101 (2009).

107. Friedrich, R., Peinke, J., Sahimi, M. & Tabar, M. R. R. Approaching complexity by stochastic methods: From biological systems to turbulence. *Physics Reports* vol. 506, 87–162 (2011).

108. Muñoz-Gil, G. *et al.* AnDi: The anomalous diffusion challenge. *arXiv.* arXiv: 2003.12036 (2020).

109. Pigolotti, S., Neri, I., Roldán, É. & Jülicher, F. Generic properties of stochastic entropy production. *Physical review letters* vol. 119, 140604 (2017).

110. Dabelow, L., Bo, S. & Eichhorn, R. Irreversibility in active matter systems: Fluctuation theorem and mutual information. *Physical Review X* vol. 9, 021009 (2019).

111. Shankar, S. & Marchetti, M. C. Hidden entropy production and work fluctuations in an ideal active gas. *Physical Review E* vol. 98, 020604 (2018).

112. Loos, S. A. & Klapp, S. H. Thermodynamic implications of non-reciprocity. *arXiv preprint arXiv:2008.00894* (2020).

113. Chaki, S. & Chakrabarti, R. Enhanced diffusion, swelling, and slow reconfiguration of a single chain in non-Gaussian active bath. *The Journal of chemical physics* vol. 150, 094902 (2019).

114. Sevilla, F. J., Arzola, A. V. & Cital, E. P. Stationary superstatistics distributions of trapped run-and-tumble particles. *Physical Review E* vol. 99, 012145 (2019).

115. Chaki, S. & Chakrabarti, R. Escape of a passive particle from an activity-induced energy landscape: emergence of slow and fast effective diffusion. *Soft Matter* vol. 16, 7103–7115 (2020).

116. Goswami, K. Heat fluctuation of a harmonically trapped particle in an active bath. *Physical Review E* vol. 99, 012112 (2019).

117. Loos, S. A., Hermann, S. M. & Klapp, S. H. Non-reciprocal hidden degrees of freedom: A unifying perspective on memory, feedback, and activity. *arXiv preprint arXiv:1910.08372* (2019).

118. Krishnamurthy, S., Ghosh, S., Chatterji, D., Ganapathy, R. & Sood, A. A Micrometer-sized Heat Engine Operating Between Bacterial Reservoirs. *arXiv preprint arXiv:1601.03130* (2016).

Acknowledgements

I would like to thank to my supervisor Giovanni Volpe for his great supervision as well as all of my colleagues. In addition, I would like to thank to all of my collaborators that made all of the work that is explained in this thesis possible. Finally, I would like to thank my friends, my family and my fiancée for their support during the time of my Ph.D. studies.